SEICHE EXCITATION IN A COASTAL BAY BY EDGE WAVES TRAVELLING ON THE CONTINENTAL SHELF.

by

DAVID DOUGLAS LEMON

B. Sc., University of British Columbia, 1972

A THESIS SUBMITTED IN PARTIAL FULFILMENT OF

THE REQUIREMENTS FOR THE DEGREE OF

MASTER OF SCIENCE

in the Department

of

PHYSICS

and the Institute of Oceanography

We accept this thesis as conforming to the required standard.

THE UNIVERSITY OF BRITISH COLUMBIA

AUGUST, 1975

In presenting this thesis in partial fulfilment of the requirements for an advanced degree at the University of British Columbia, I agree that the Library shall make it freely available for reference and study. I further agree that permission for extensive copying of this thesis for scholarly purposes may be granted by the Head of my Department or by his representatives. It is understood that copying or publication of this thesis for financial gain shall not be allowed without my written permission.

Department of Physics

The University of British Columbia
2075 Wesbrook Place
Vancouver, Canada
V6T 1W5

Date 22 August, 1975.

ABSTRACT

Short period ($\leq$ 1 hour) oscillations are often seen superimposed on tidal curves at Port Renfrew, B.C. In order to determine the nature of these oscillations, time-series of sea-level variation were obtained in Port San Juan; their analysis revealed energy peaks at periods of 34.7 min. and 13.5 min. A theoretical model of wave excitation of a basin of variable depth fitted to Port San Juan by edge waves travelling on the shelf accounts reasonably for the observed frequencies. Bottom friction was taken into account to investigate the dependence of seiche amplitude on the amplitude of the shelf waves.

TABLE OF CONTENTS

LIST OF TABLES

LIST OF FIGURES

Page

ACKNOWLEDGEMENTS

I would like to thank my supervisor Dr. P. H. LeBlond, for his encouragement and assistance in the writing of this thesis. I would also like to thank Dr.T.R. Osborn for his assistance, especially with the experimental part of this work. Special thanks are due to Mr. J. L. Galloway for his assistance in the design and construction of the wave gauge. I am grateful for the cooperation from all the members of the Institute of Oceanography at U.B.C.

Finally, I wish to thank the National Research Council of Canada for supporting me personally during two years of this research.

CHAPTER 1

INTRODUCTION

The purpose of this work was to compare the results of analytic modelling of a seiche in a coastal bay to measurements of the seiche. In order to do this, a bay amenable to analytic modelling was necessary. Port San Juan is such a bay. It is situated on the west coast of Vancouver Island, near the entrance to the Strait of Juan de Fuca (see Fig. 1.1). The bay is extremely regular in plan, being rectangular with steep side walls and a gently shelving beach at the head (see Fig. 1.2). The bottom slopes regularly and smoothly from the head of the bay to the entrance. The bay is approximately 6.5 km. long, 2 km. wide and about 16 metres deep at the entrance. A tide gauge operated by the Department of the Environment (Water Management) is situated on the government wharf at the small village of Port Renfrew, about 2 (Km.) from the head of the bay on the southeast shore. Two small rivers, the San Juan River and the Gordon River enter at the head of the bay. The entrance of the bay looks out into the open Pacific past Cape Flattery and is exposed to surf from the open ocean.

Port San Juan was very well suited to analytic modelling because of its extremely regular shape. The other requirement of this study was that seiches should exist there. The government tide gauge did show evidence of seiche action.

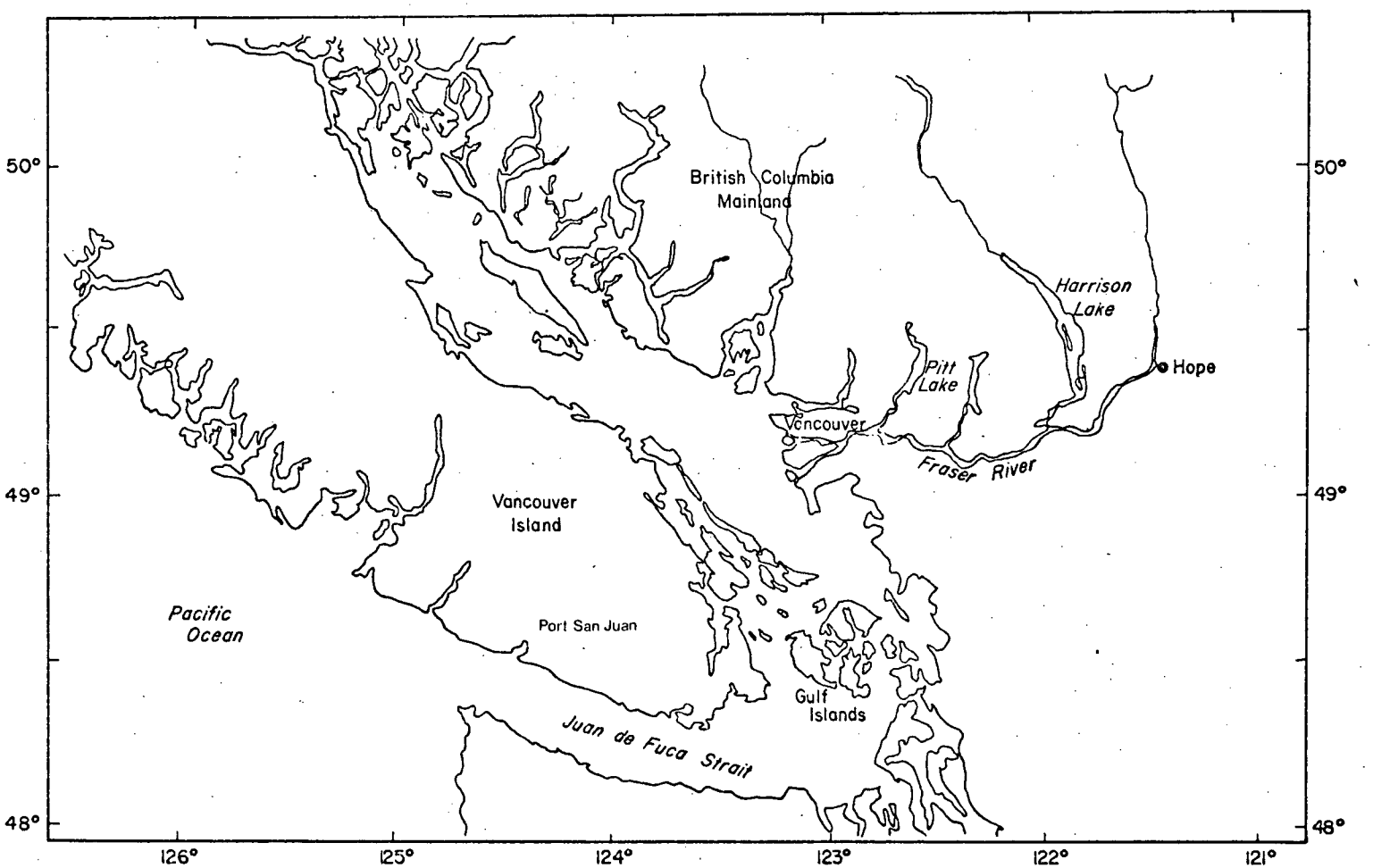

Fig. 1.1 The Strait of Juan de Fuca and Port San Juan.

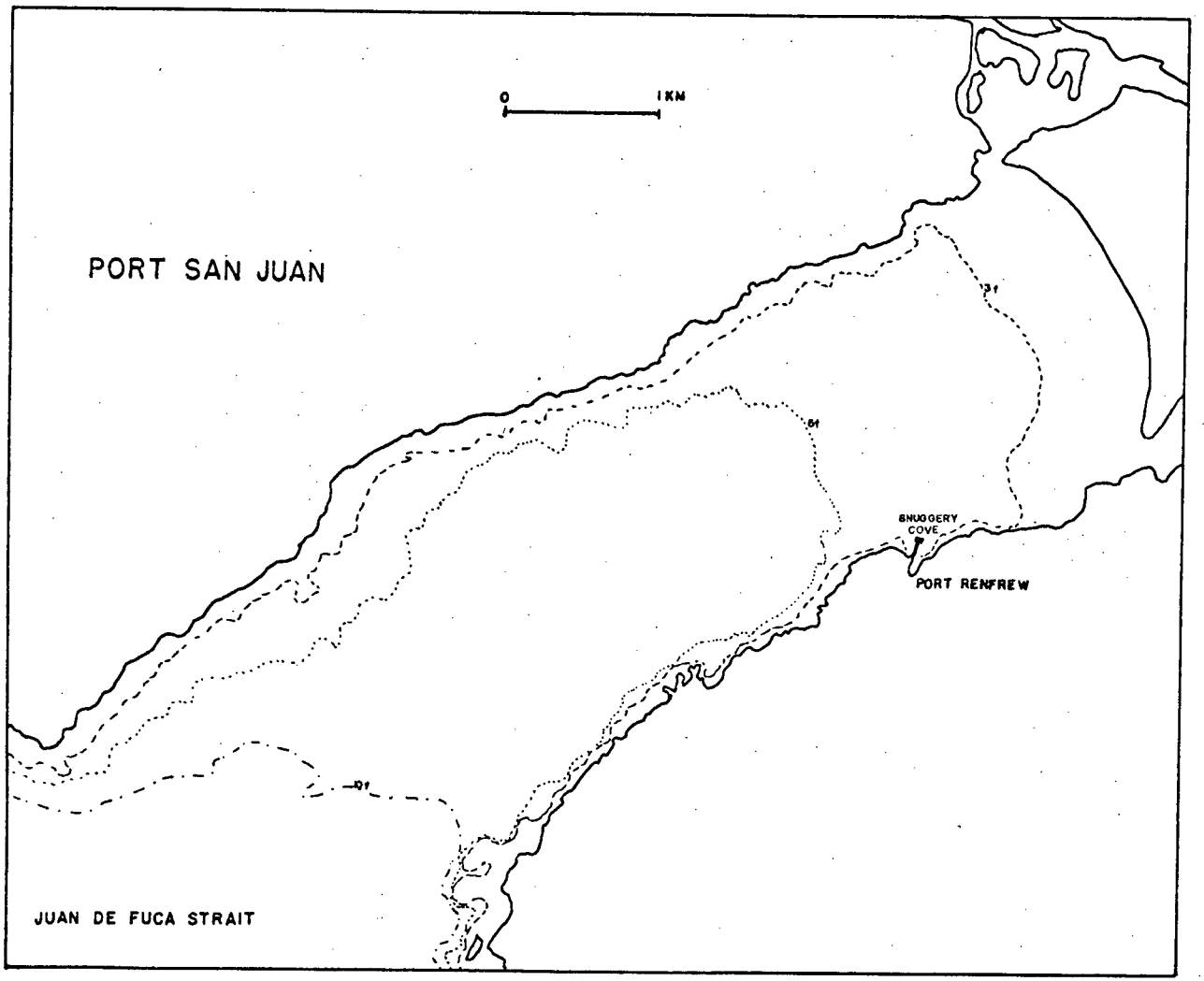

Fig. 1.2 Port San Juan. Measurements were taken at the government wharf in Snuggery Cove.

CHAPTER 2

DATA

2.1) Prior Evidence of Seiches

Evidence of seiche action in Port San Juan bay exists on the records of the government tide gauge. (S.O. Wigen, Personal communication) An example of these motions as detected by the government gauge is shown in Fig. 2.1. The gauge in use at Port Renfrew is a very simple instrument, consisting of a clock-work-driven chart recorder which is marked by a pen connected to a float and a counterweight. The float is suspended inside a stilling well consisting of a long piece of pipe, about 12 inches in diameter which is attached vertically to the wharf pilings. The stilling well does not perform its filtering function very well, with the result that the record is contaminated by high frequency noise produced by surface waves. Other examples of the occurence of the seiche are shown in Fig. 2.2. Visual examination of the record reveals two distinct periods for the seiche: one of the order of 35 minutes, and one of the order of 15 minutes.

Investigation of all these records for the year 1973 revealed no correlation between the occurrence of seiches and the phase of tidal motions. The seiche may occur on any phase of the tide; many tidal cycles may go by without any appearance of the seiche at all. Neither is there any obvious correlation with storm activity [illegible] the width of the noise in the re[illegible]

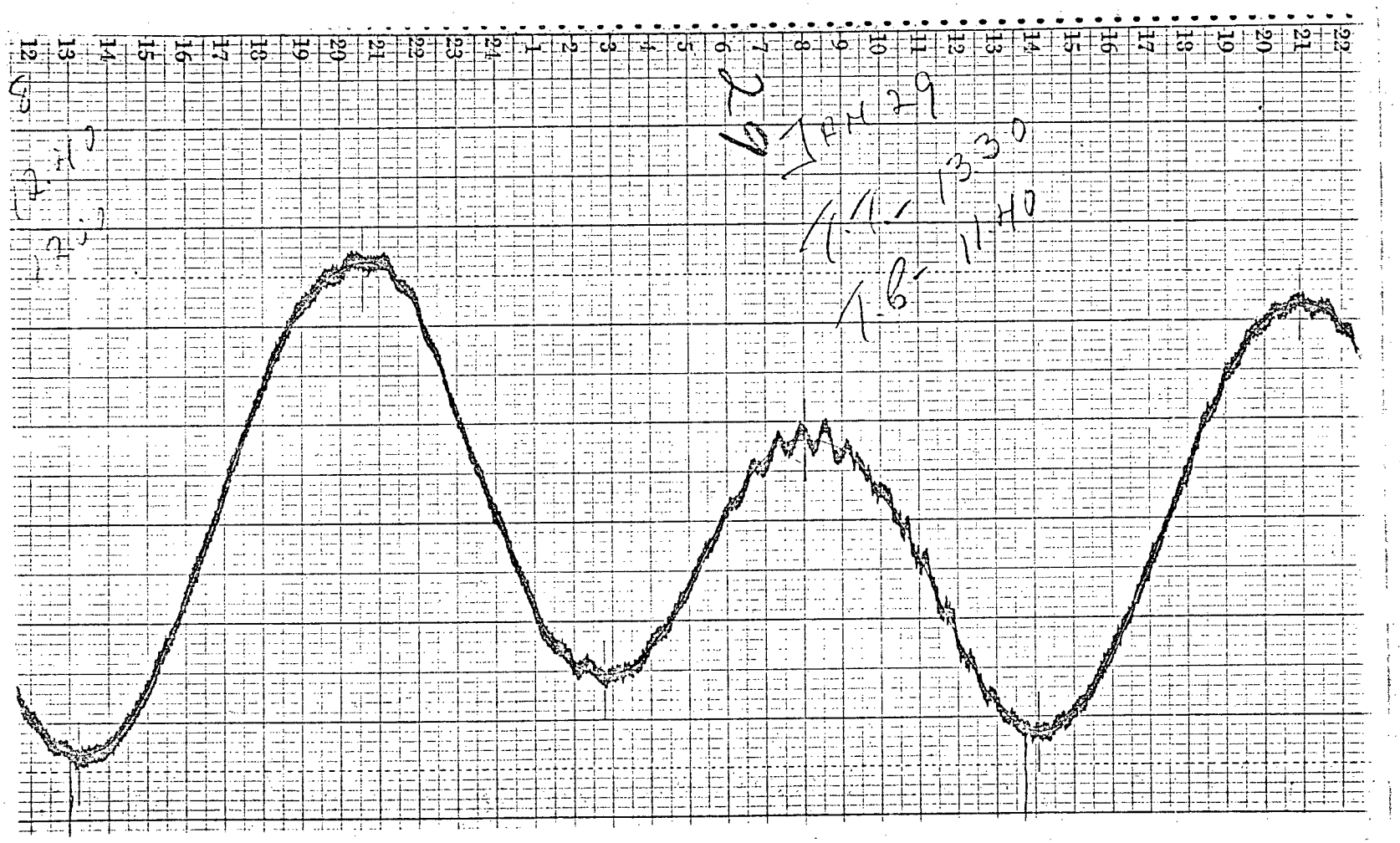

Fig. 2.1 Seiche action on the government tide gauge, 29 January 1971.

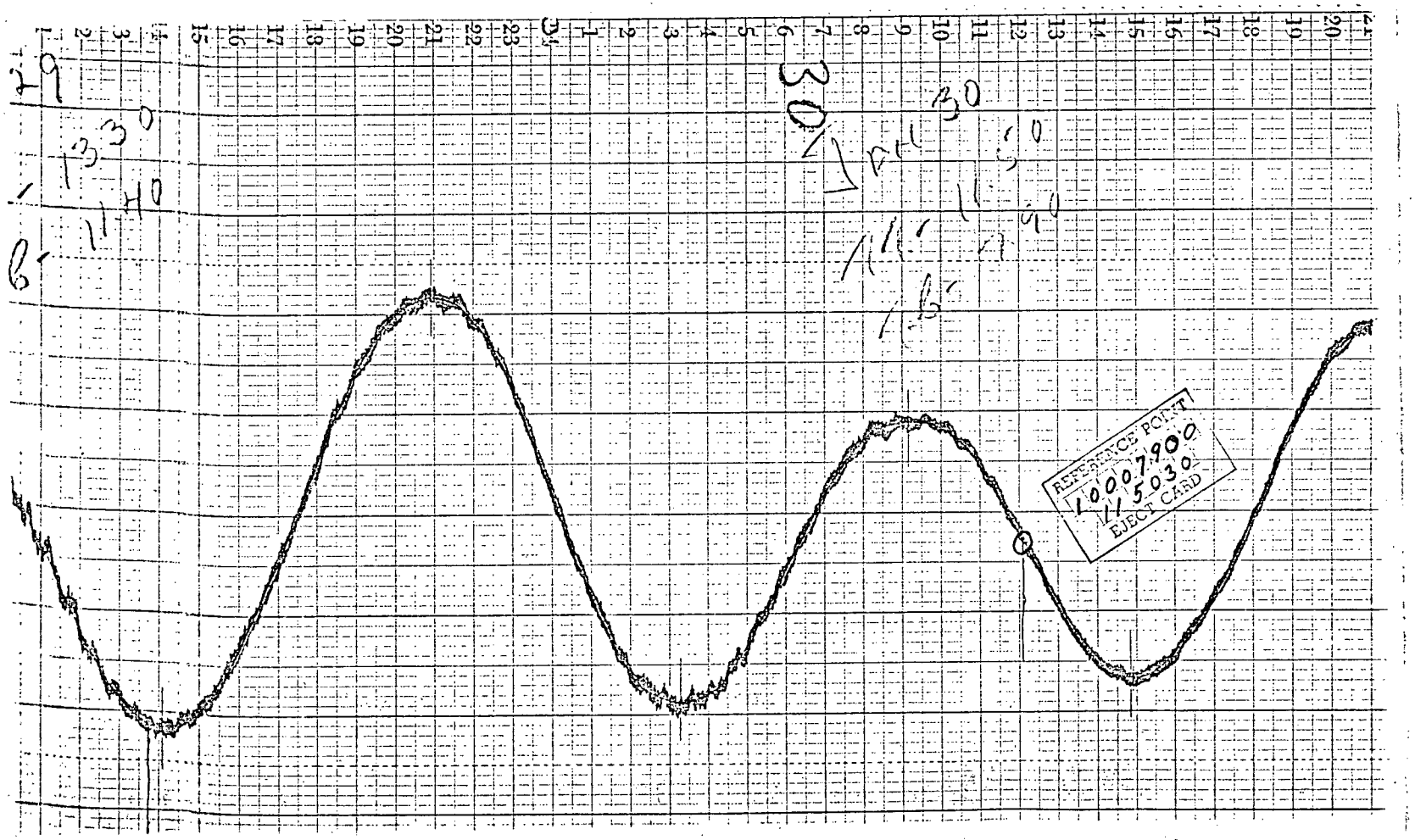

Fig. 2.2 Seiche action on government tide gauge, 30 January 1971.

(as revealed by the width of the noise on the record), although there tends to be more seiche activity in the late fall, winter and early spring than in the summer months. The seiche amplitude varies markedly as well; usually it is of the order of 5cm. The largest observed amplitude was 15 cm. The amplitude also shows no obvious correlation with tide or storm activity.

2.2) Method of Measurement.

The government tide gauge records were not suitable for making precise determinations of the period and amplitude of the seiche. Therefore a more precise measurement using another instrument designed for the purpose was deemed necessary. A bottom mounted pressure gauge, based on a design by J. L. Galloway (Galloway, 1974) using a vibrotron transducer was built to measure the seiche. The instrument was originally designed as a shallow-water tide gauge; some modifications were necessary to enable it to measure seiches, but the basic form of the instrument remained the same. Details of the design and operation of the instrument may be found in Appendix C.

The record from the instrument was a time-varying analogue voltage. In order to achieve the necessary precision of measurement over the large tidal range, a scale expansion technique was used. When the change in water level exceeded the full scale range of the

scale expansion technique

instrument output, the signal would wrap around and return to zero, effectively keeping only the least significant portion of the signal. Thus a rising and then falling tide would produce signals like that in Fig. 2.3. These wraparounds could then be removed after the record was digitized.

The instrument had four output channels; two low-frequency channels incorporating a filter to remove the surface waves, and two channels with a high sampling frequency which recorded surface waves. Both groups incorporated a high and low resolution channel. The low-resolution channels were designed to operate without wraparounds. They were included in case the wraparounds could not be removed later; since wraparounds were removed, the low resolution channels were not used in the analysis.

2.2.3) Data Collection

I collected the field data for the study at Port Renfrew on 26, 27, and 28 February 1974, installing the instrument on the government wharf near the tide gauge, (see Fig. 1.2), where 110 volt AC line power was available. The trailer containing the electronics was left parked on the wharf, and the sensor head was lowered on a heavily weighted frame down to the bottom. The water depth over the instrument at high tide was 5.95 metres.

The output from the instrument was recorded on a 2-track Brush recorder as well as the magnetic tape, to give a visual

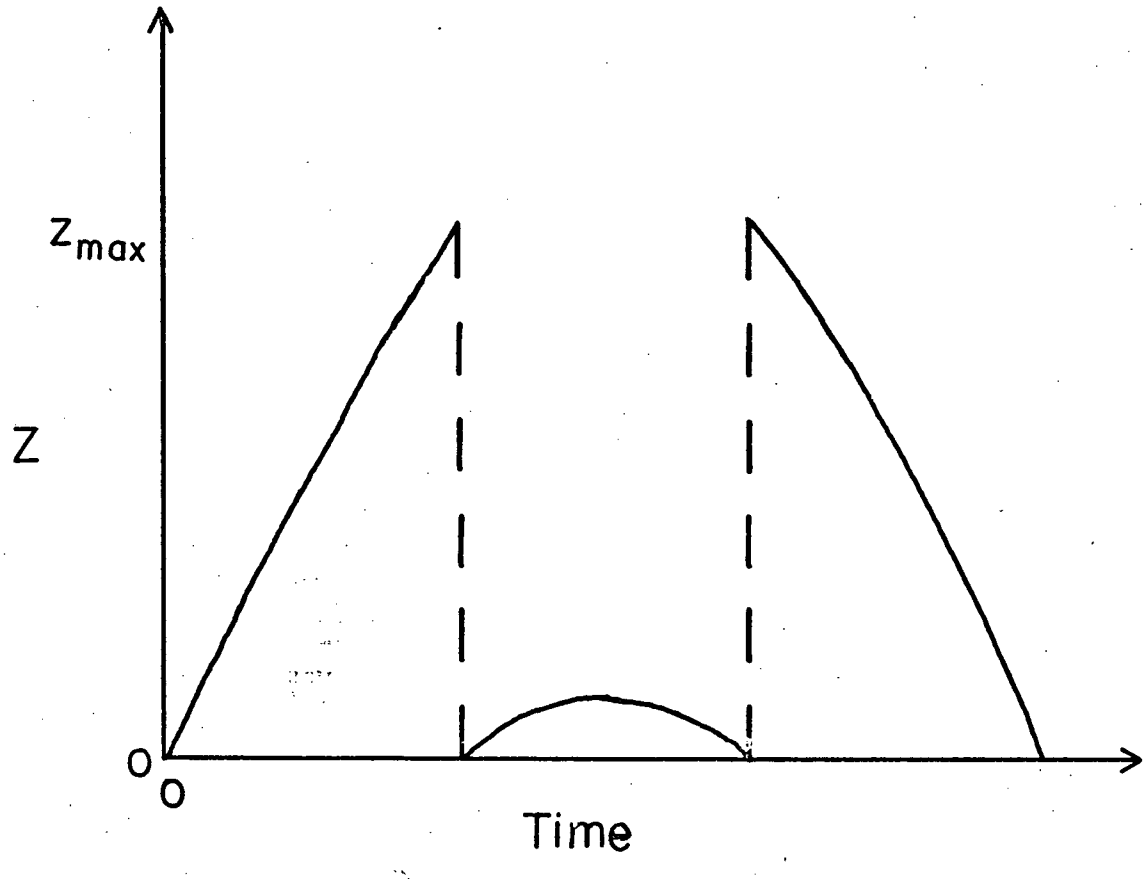

Fig. 2.3 The wraparound technique for scale expansion .

check on the instrument's operation. After the pressure head had been lowered, inspection of the government tide gauge showed that no seiches were happening, so I did not immediately turn on the recorder.

The recorder was turned on at 0600 27 February when seiche motions appeared on the government tide gauge. Recording continued, interrupted only by tape changes every 6 hours, until 1915 27 February when a general power failure occured throughout Port Renfrew. A severe storm going on at the time had blown a tree across the power lines.

Power was restored at 2315 and recording continued. At some time between 0445 February 28 and 1030 February 28 the tape recorder failed and I was unable to repair it with the equipment at hand. Since I had 13 hours of good data with the seiche occurring, I returned to Vancouver. Data collection was finished.

2.4) Time Series Processing:

The time series obtained from the above measurements could not be directly used for the computation of a power spectrum of the series. As it was stored in analogue form on several tapes it was first necessary to digitize it, and then to mate the individual records into one long record. It was then necessary to remove the wraparounds, calibrate the digitized record and remove the tidal trend. The details of these operations are

described below.

a) Digitization and record patching:

The records were digitized using the A-D system on the Institute of Oceanography PDP-12 computer. The system accepts analogue signals between +2 and -2 volts and produces a digital output signal between -511 and +512 which is written out on 9 track computer tape. The sampling rate may be adjusted to any value up to 16000 $sec.^{-1}$

The record tapes were played separately and digitized into separate datafiles. Only the two high-resolution channels were used in the actual analysis. The playback was done at 16 times the recording speed, and the digitization rate was adjusted accordingly. On Channel 2 the sampling rate of 2 Hz., when replayed at the higher rate, produced a signal varying in real time at 32 Hz (=2 x 16 Hz.). Since the digitization system works only at certain fixed frequencies, the digitization was carried out at the closest available frequency, which was 50 Hz. Similarly, Channel 4, which sampled at 1/21 Hz., was digitized at 1.5 Hz.

Each channel had a + and - full scale signal recorded at the beginning for calibration purpose. After adjustment of the tape recorder output amplifiers, these signals were digitized to give the scale for each channel which was as below in table I.

Table I

Digitizer scale constants.

Channel	+ FS	-FS
4	429	-431
2	425	-427

These maxima were set somewhat below the full range of the digitizer in order to avoid saturating the system.

The next problem was to fit the individual tapes together, fill the gaps between them, and then remove the wraparounds. Since the time between tapes was known I filled these intertape gaps by linearly interpolating the correct number of values ($n = \Delta t/dt$; dt= digitization period; Δt= gap time) between the last reading from one tape and the first reading on the next.

Then the wraparounds were removed numerically. A criterion of 70% of full scale was taken to represent a wraparound, and the time series were then run through a computer program which automatically added or subtracted full scale to all values following a wraparound. The result of these treatments was a relatively clean time series with only minor data gaps (9 minutes out of 755, or gaps of 1.2% of the records.)

Channel 4 had a total of 4225 points, 10.72 seconds apart, making a total record length of 45,292 seconds or 12.581 hours.

Channel 2 produced 131,689 points, 0.32 seconds apart, making a total record length of 42,141 seconds. Both records had to be truncated somewhat in order to facilitate the use of the Fast Fourier Transform program. Channel 2 was cut back to 4096 points for a total record length of 43,909 sec. (12.20 hrs.) and channel 4 was reduced to 131,072 points for a total record length of 41,943 sec. (11.65 hrs.)

b) Calibration

The vibrotron response is not linear with frequency as equation C.1 in Appendix C shows. The departure from linearity is small, but nevertheless a calibration of the results seemed to be in order. Instead of individually calibrating each part of the instrument, I decided to treat the entire system (including the digitizer) as one black box, and calibrate the output trace itself.

I decided to calibrate the instrument against the government tide gauge. The non-linearities in the vibrotron responses are sufficiently small that they will only show up over large depth ranges. Within smaller depth excursions, the response of the instrument should be linear.

To remove the effect of surface waves, half-hour averages of the channel 4 output were plotted against the appropriate values from the government tide gauge trace.

Fig. 2.4 shows a plot of the actual water depth vs. the digitizer counts for channel 4 over the period of measurement. The vertical error bars arise from errors in estimating the position of the government gauge trace and are equal to 1/2 the width of the trace. Fig 2.5 shows the relation between counts for channel 2 and channel 4. The curve in Fig 2.4 was fitted with a cubic, resulting in the following calibration equation for channel 4

$$Z=18.78 + 1.97 \times 10^{-2}C + 2.9 \times 10^{-7}C^2 + 9.18 \times 10^{-11} C^3$$

where C is the count and Z is the water depth in feet. The count for channel 2 is related to the count for channel 4 by

$$C2 = 0.403C4 + 35.87$$

where C2 = channel 2 count

C4 = channel 4 count

These results show that the instrument sensitivity changes slightly with the total depth of the water. Table II lists the sensitivity as a function of the total water depth:

Table II

Sensitivity as a function of depth.

Depth (feet)	Sensitivity (mm./ count)
18.75	0.598
17.31	0.510
16.01	0.525

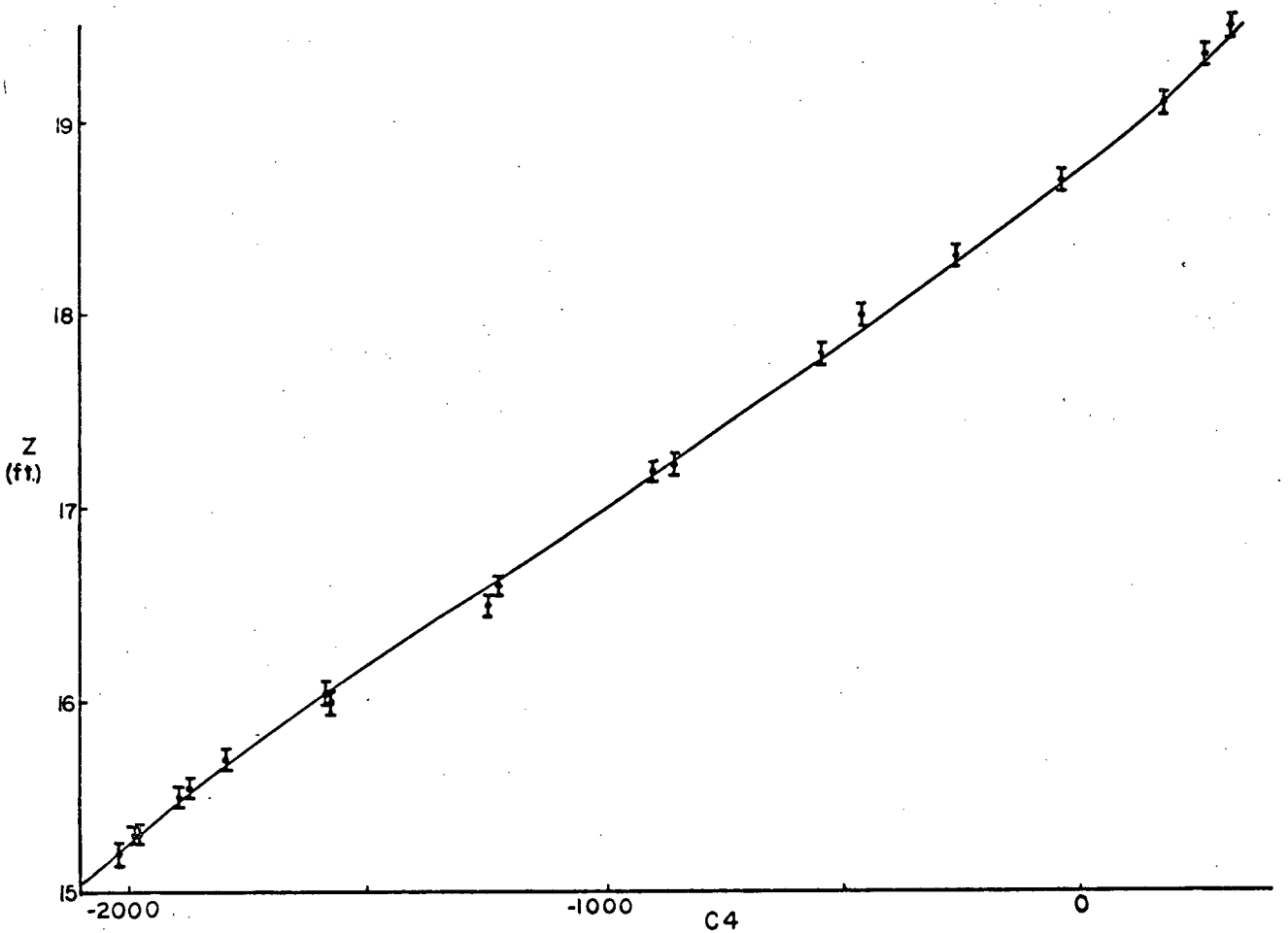

Fig. 2.4 The calibration curve for channel 4 of water depth vs. digitizer count.

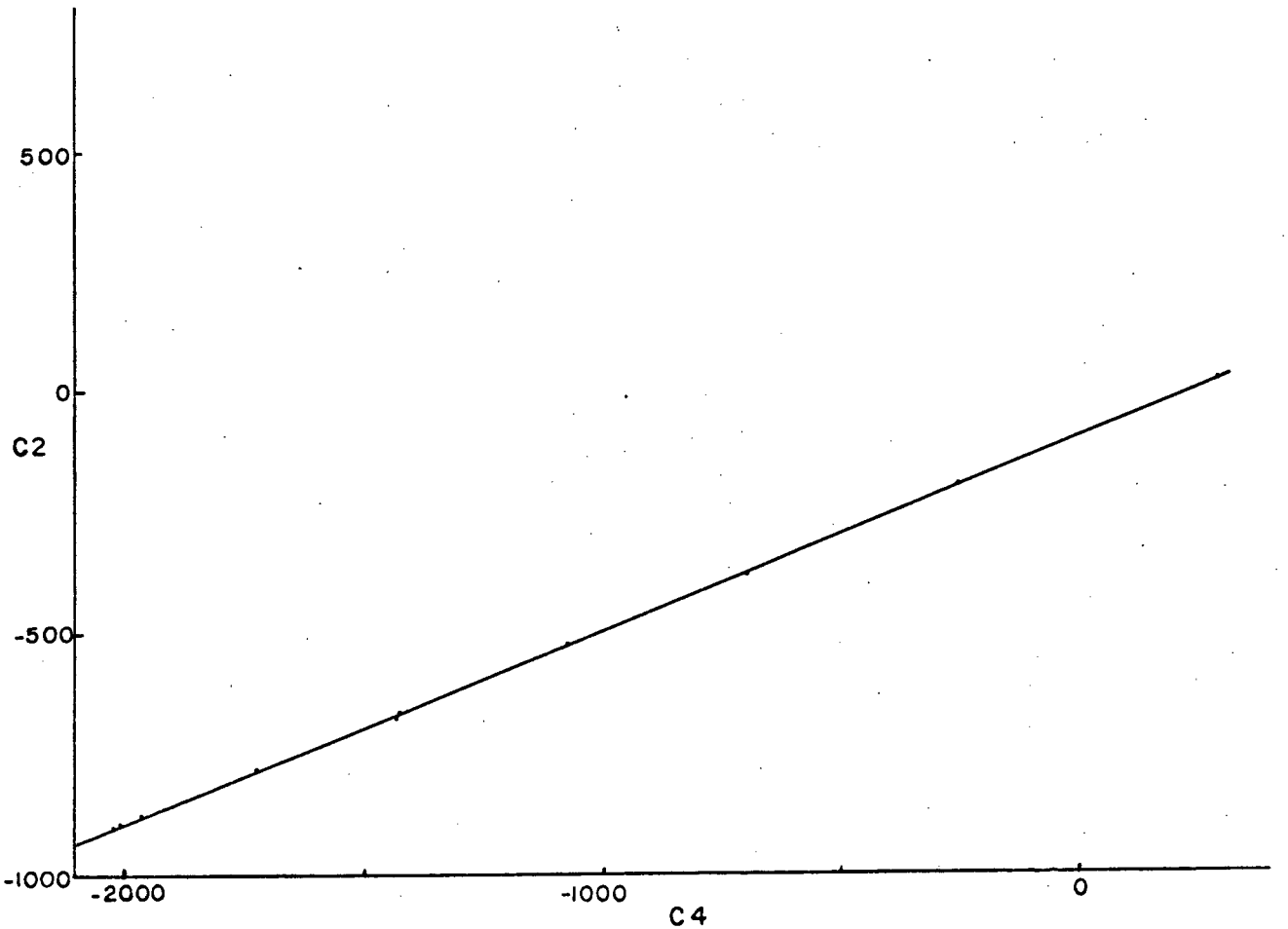

Fig. 2.5 The calibration for channel 2. The plot shows counts for channel 2 vs. counts for channel 4.

Note that these counts are counts from the digitizer output, not the internal instrument counts mentioned in Appendix C. Since these are smaller, the net effect is that the digitizer count always changes by at least three.

c) Detrending

Fig. 2.6 shows the time series resulting from channel 4. The high-frequency oscillations are partially filtered surface waves (see Appendix C for the filtering process). The seiche is visible as the longer period oscillations superimposed on the main tidal curve. The tidal curve presents a major problem in analyzing the data. The purpose of the measurement was to obtain a more precise measurement of the seiche period than that possible using the government gauge. However a spectrum of the curve shown in Fig. 2.6 would not yield any information about the seiche beacuse of the tidal trend. The record is far too short to resolve the tidal peaks properly, with the result that the low frequency end of the spectrum is obscured including the frequency band containing the seiche frequencies. This may be seen in Fig. 2.7 which shows a power spectrum computed from the trace shown in Fig. 2.6. Note that all detail is obscured in the low frequency region of the spectrum, i.e. at frequencies less than 5.6×10^{-3} Hz.

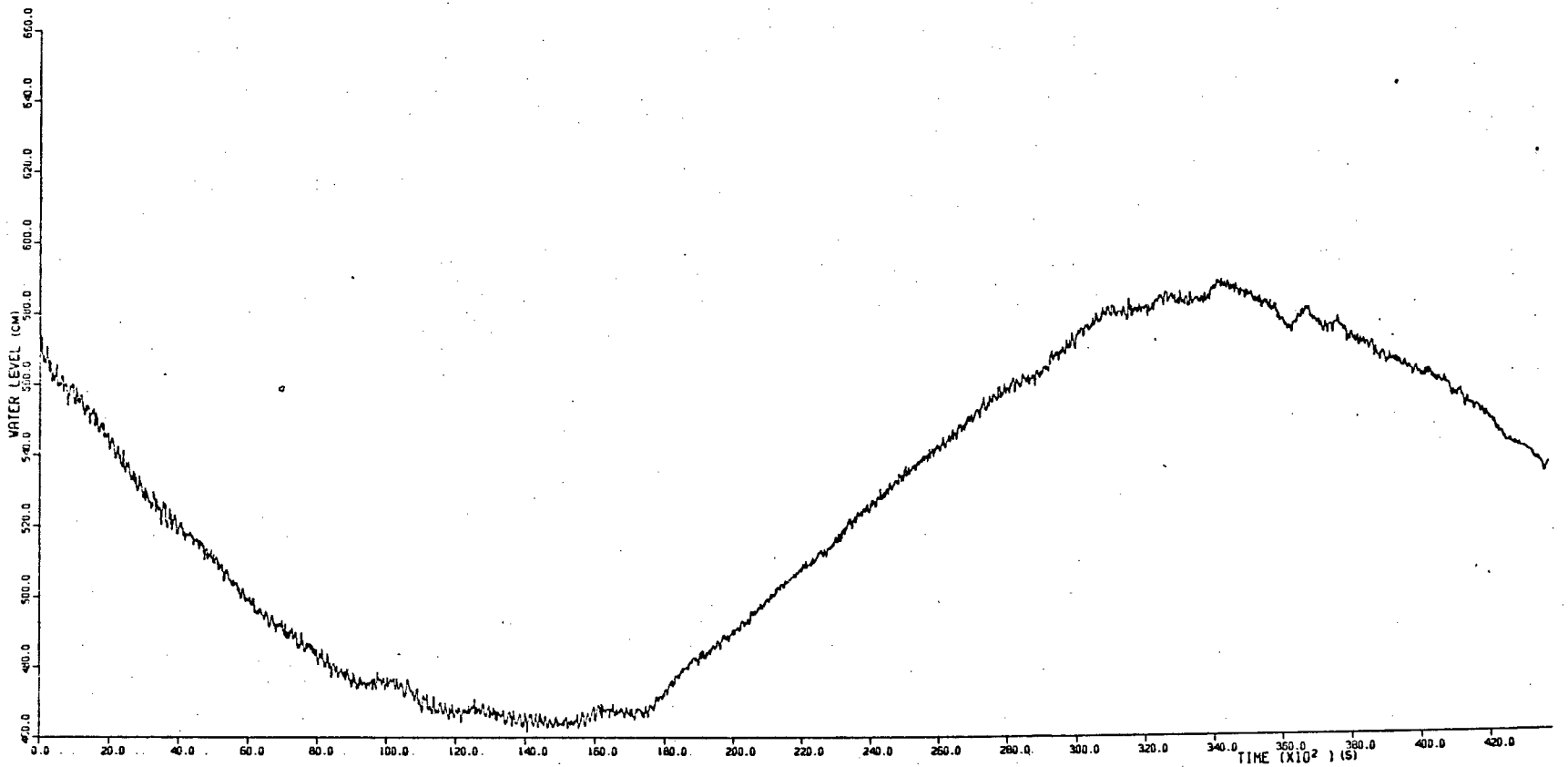

Fig. 2.6 Water depth vs. time from channel 4.

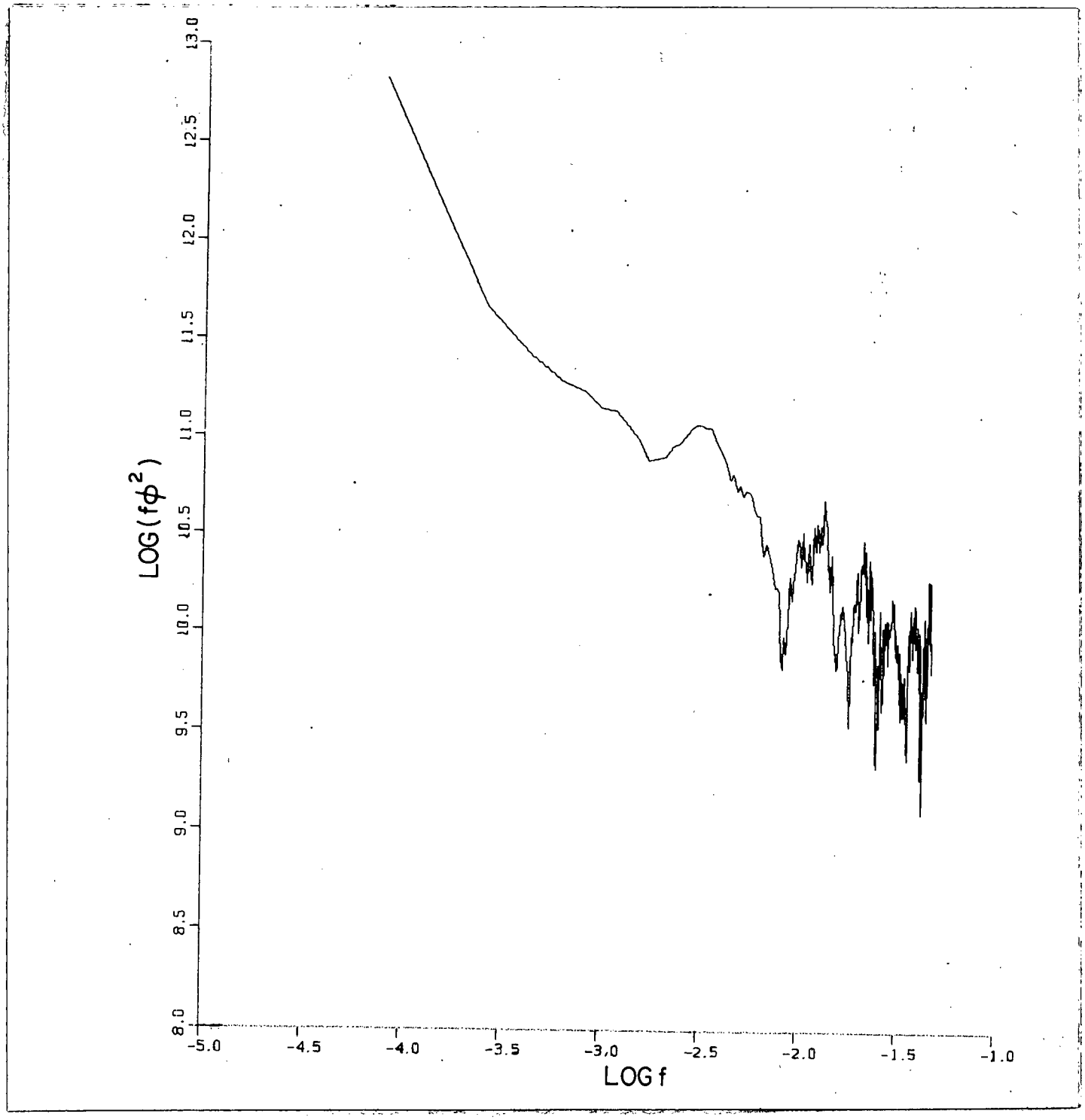

Fig. 2.7 The power spectrum of the raw time series in Fig. 2.6.

Some method must therefore be found to remove the effects of the trend from the very low frequencies. This effect arises because the record is not long enough to resolve the tidal motions. Digital filters of the type which eliminate undesired Fourier coefficients, and then retransform the spectrum were not suitable, since this would have destroyed the very information I was attempting to extract from the record. Any filtering had to be performed on the time series in such a manner as to preserve motions near the seiche period.

There is a class of digital filters described in Godin (1972) which work on the time series itself by taking successive differences between values, ($S_1^M(\sigma)$, in Godin's notation). These however usually cut off everything below half the Nyquist frequency, which in this case meant that only the surface wind-waves would survive the filtering process. Therefore, some other method of removing the tidal trend had to be found.

Since the trend is tidal in origin, the best method of removing it appeared to be to take the predicted tide for Port Renfrew and subtract it from the time series data. If the amplitudes and phases of the various constituents of the tide at a port are known, then it is possible to predict the tide there from the formula

$$h = H_o + \sum_{\substack{\text{all} \\ \text{constituents}}} f\, H \cos[\, at + (V_o + u) - \kappa\,] \quad , \qquad (2.3)$$

(Schureman, 1958), where

h= the tide height at time t,

H_0= the mean water height above datum,

H= the amplitude of a tidal constituent,

f= a factor reducing the mean amplitude H to the year of prediction,

a= the speed of the constituent of amlitude H,

t= the time measured from starting point of predictions,

(V_0+u)= The value of equilibrium argument of the constituent of ampitude H when t=0, at Greenwich,

k= the phase of the constituent with respect to Greenwich (in Canadian System).

The values of f, a and $(V_o + u)$ are tabulated (Schureman, 1958) and may be found for any starting time. The amplitudes and phases for Port Renfrew are shown in Table III. The seven largest constituents (and the only ones used are) M2,K1, O1,S2,N2,P1, and K2. The tide at Port Renfrew for the period of measurement was then calculated from (2.3) for the period of observations, producing the curve shown in Fig. 2.8. This was subtracted from the original time series to produce a tidally corrected curve, shown in Fig. 2.9.

A rather large residual was left. There was sufficient energy contained in this residual that it was necessary to remove it as well as the tide, before the peaks due to the seiche could be made clearly visible. Therefore I decided to try to fit a curve to the overall trend in the data. I tried two different methods, in order to have some comparison between them. This might therefore help to keep a check on articial effects introduced by the fitting.

Table III

Tidal constituents at Port Renfrew.

Name	Amplitude (m)	Phase (°)
M2	2.351	9.3
K1	1.492	134.4
O1	0.918	122.9
S2	0.656	29.1
N2	0.488	354.0
P1	0.488	133.5
K2	0.174	6.3

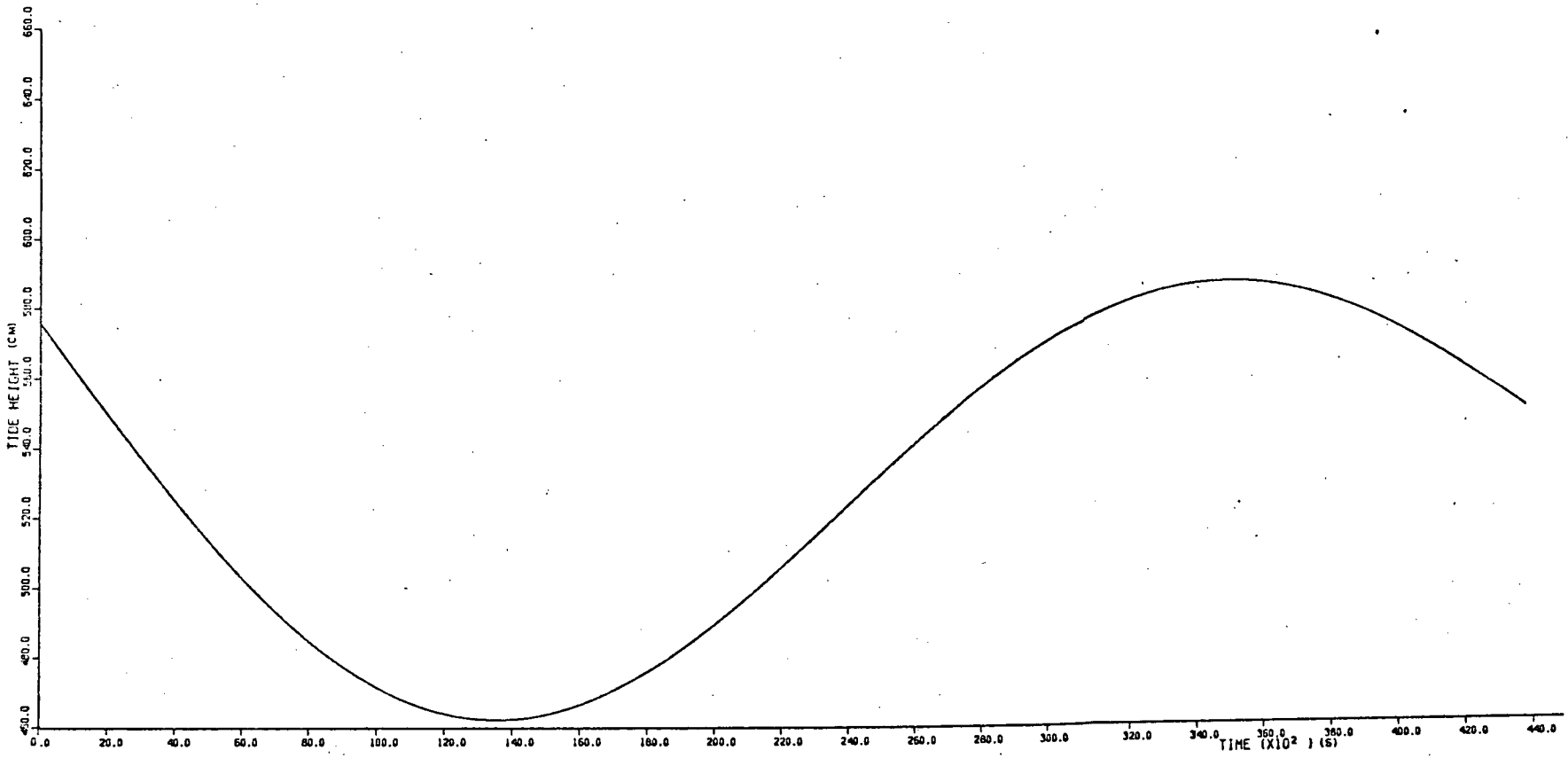

Fig. 2.8 The predicted tide at Port Renfrew for the period of seiche measurement: 0600 - 1915 27 February 1974.

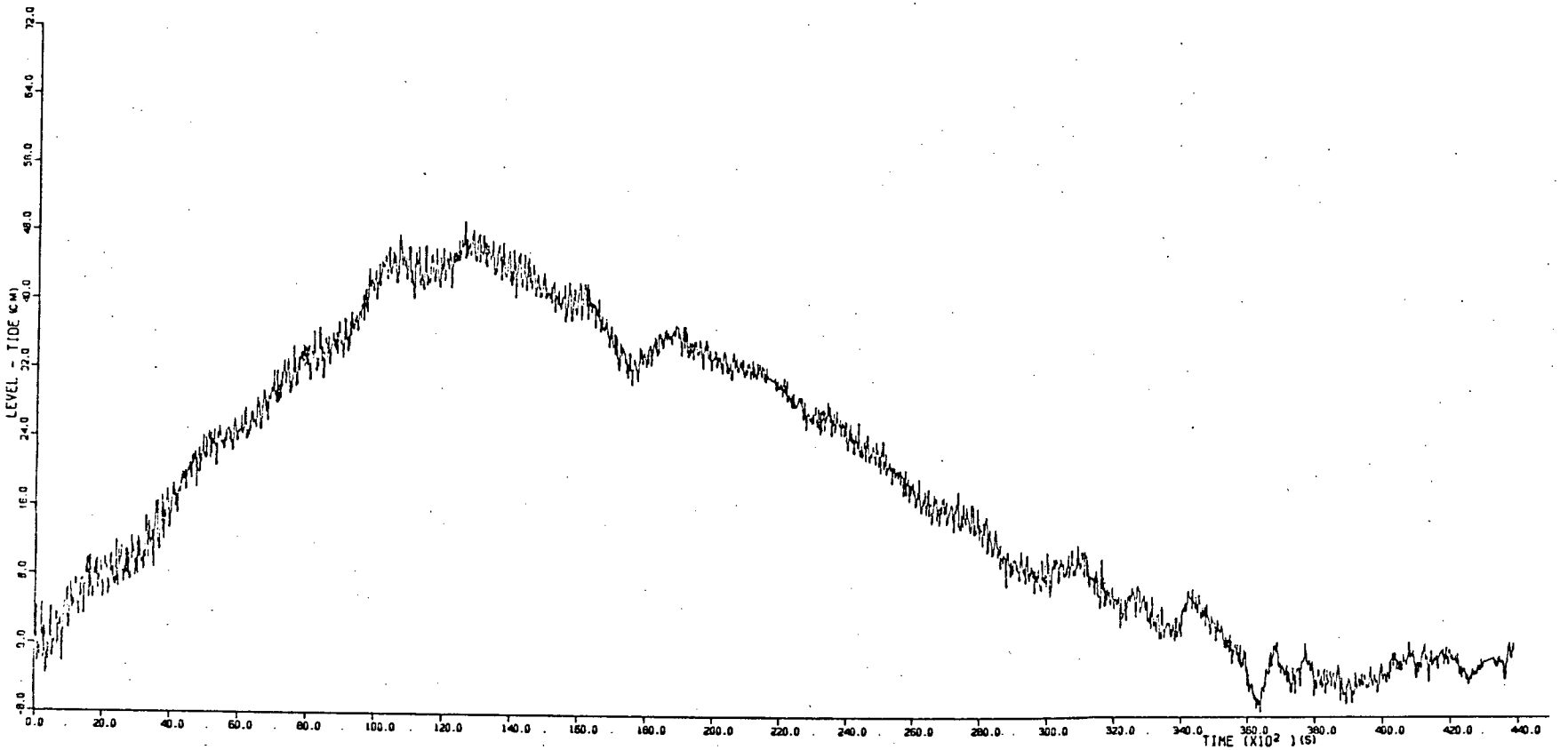

Fig. 2.9 The time series from Fig. 2.6, corrected for the tide.

The first detrending method chosen was a polynomial fit using the U.B.C. Computing Centre Program ULQF (Bird, 1974). The fitting had to be done to the large scale trend, without obscuring the seiche motions. There were 4096 data points in the time series. These points were averaged in groups of 100, to produce 40 points representing the long-term trend in the time series. The polynomial fitting program was then run on this time series. The program employs a least squares fitting technique to find the best fit polynomial of degree less than or equal to an externally supplied maximum degree. Since I did not want to destroy the seiche information, a polynomial of relatively low degree was necessary. I ran the program with the maximum degree set at 5. The program chose a cubic as the best fit. This polynomial was then used to generate a new time series, one point for each in the original series. This new series was subtracted from the old and the result was the corrected time series shown in Fig. 2.10.

The other method used was a spline fitting technique with error (Bird, 1974). This program uses a spline fitting technique to fit a curve to a series of points with errors. Therefore I let the surface wave and seiche amplitude be errors in the points (allowing an error of 7.0 cm in each point) and then ran the program to fit a correction to the trend in the series. The resulting time series is shown in Fig. 2.11.

As a further check, I then ran the polynomial fitting program on the spline-corrected time series. This time series is shown in Fig. 2.12.

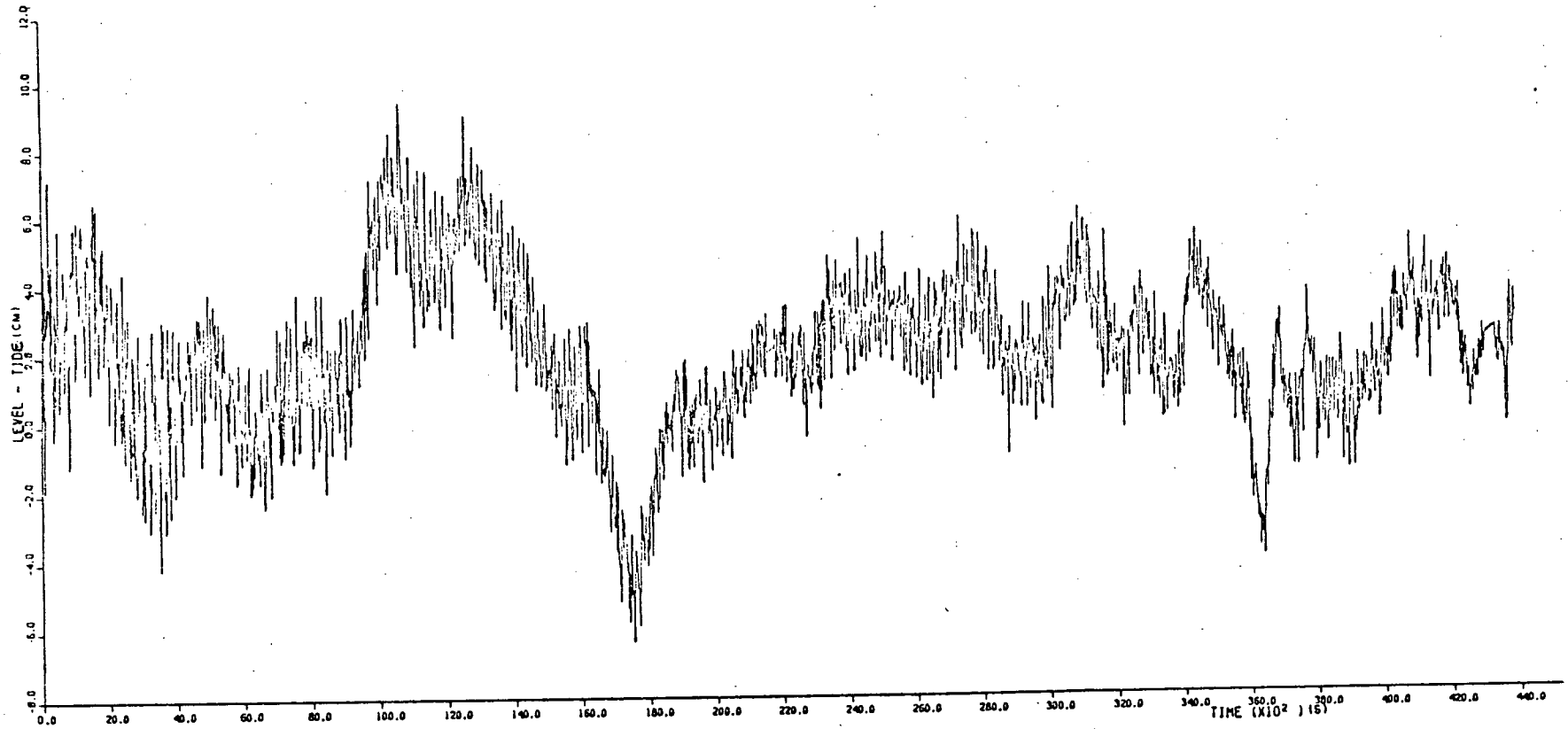

Fig. 2.10 The tidally corrected time series with a cubic fit sugtracted to remove the residual.

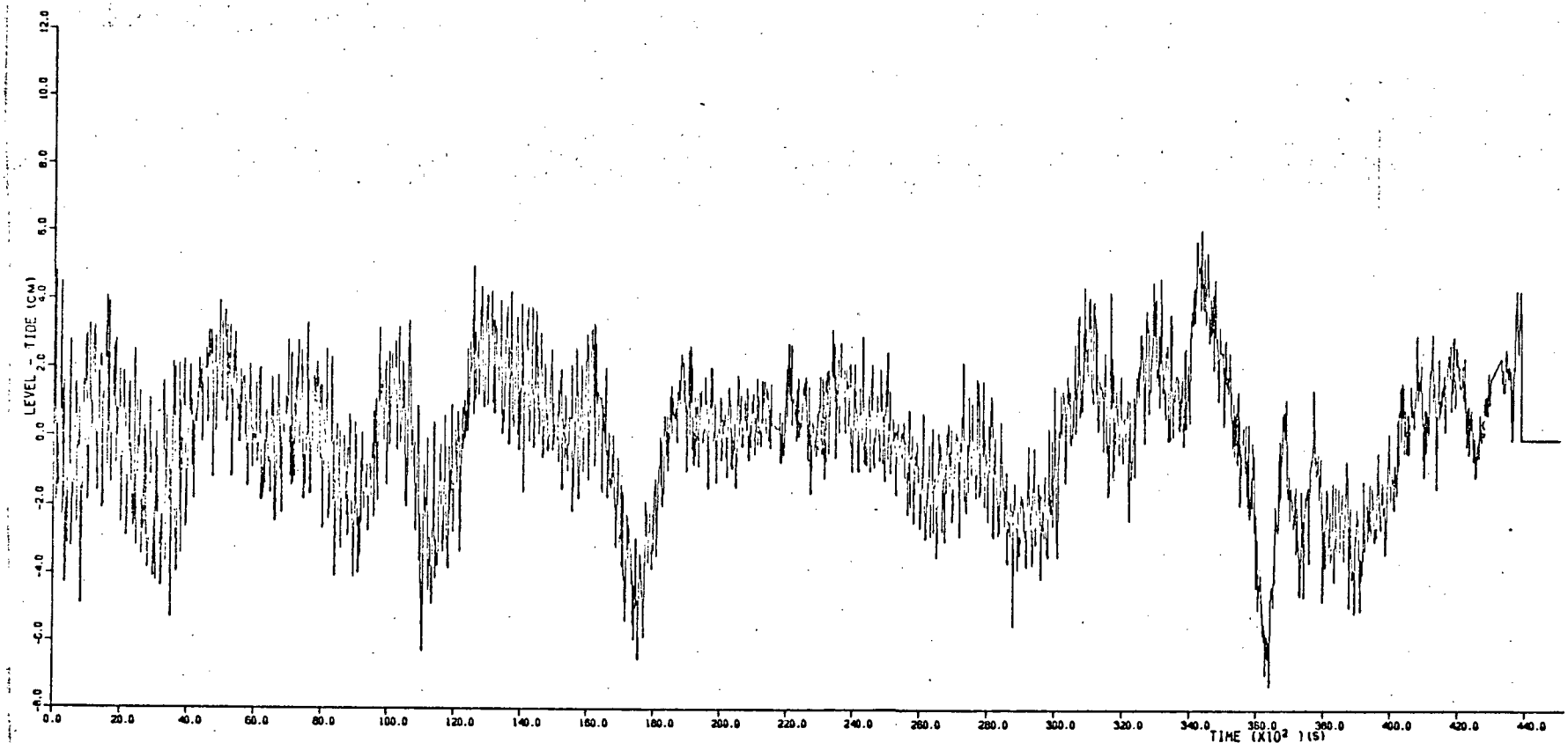

Fig. 2.11 The tidally corrected series with a spline fit subtracted to remove the residual.

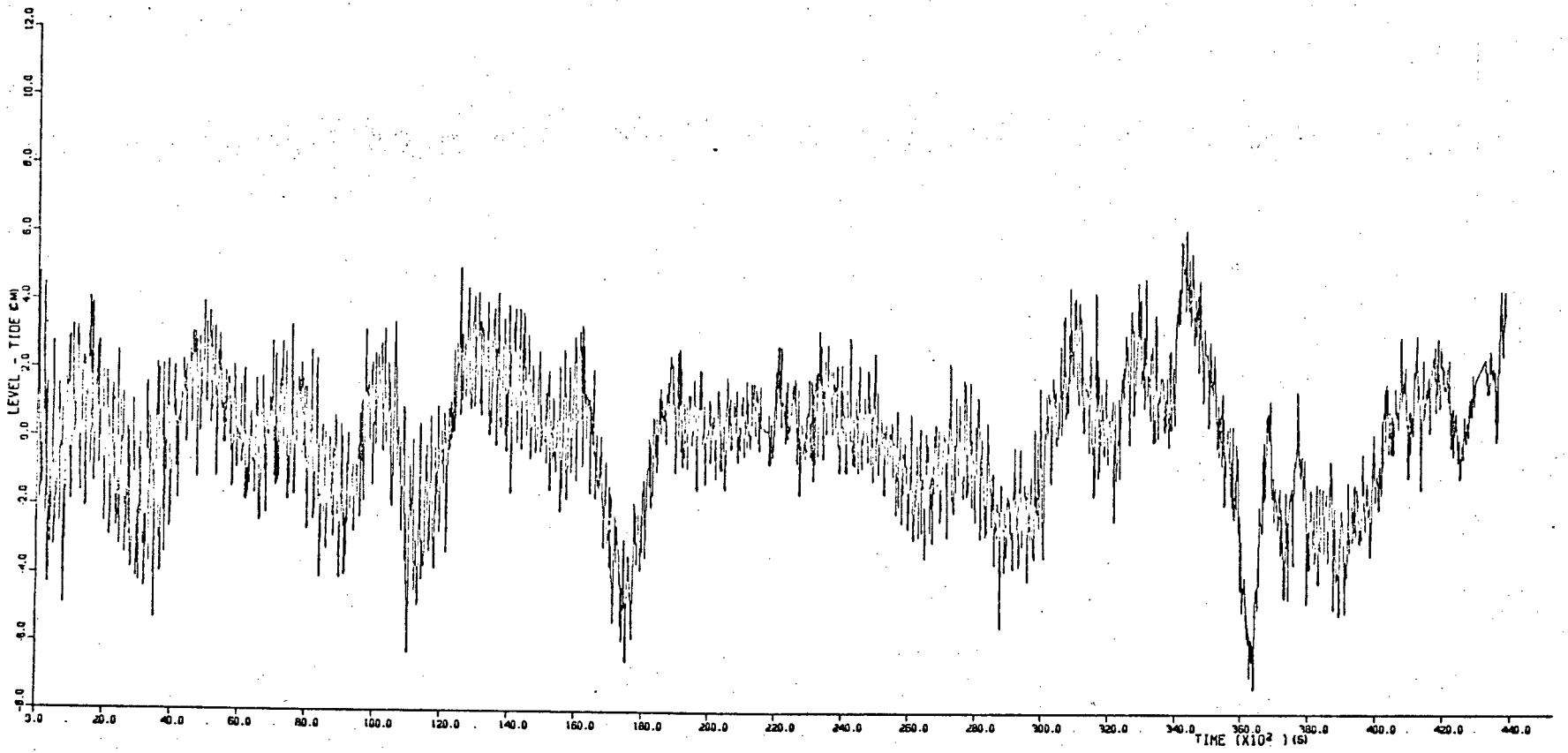

Fig. 2.12 The spline - corrected series (from Fig. 2.11) with a polynomial fit also subtracted.

5)Spectral Calculations

Spectra were calculate (for all these time series using the standard Fast Fourier Transform algorithm is the U.B.C Computing Centre program FOURT (Froese, 1970).

Fig. 2.13 show the transform computed for the cubic-corrected time series shown in 2.10. Log ($f\phi^2$) is plotted vs. log f. Each point on the plot is composed of a 4 point average of the Fourier coefficients, giving a somewhat smoothed plot.

Figs. 2.14 and 2.15 show the spectra for the spline and spline-polynomial corrected series in Figs. 2.11 and 2.12 respectively.

It is necessary to perform smoothing operations on the spectrum in order to obtain consistent spectral estimates. For a Gaussian variable, a power spectrum computed by direct Fourier tansform methods results in a normalized standard error in each estimate of E_r=1. (Bendat & Piersol, 1971).

There are two possible methods to reduce the error in each spectral estimate. One may either perform an ensemble average on spectra resulting from several time series of the same phenomenon (i.e. break a longer record into short segments and perform a spectral analysis on each short record), or one may average the spectral estimates in a given frequency band together to produce one estimate for that band. The two processes are entirely equivalent (Bendat & Piersol 1971).

The error E_r referred to above is a random error only; the averaging processes above wil reduce it by the formula

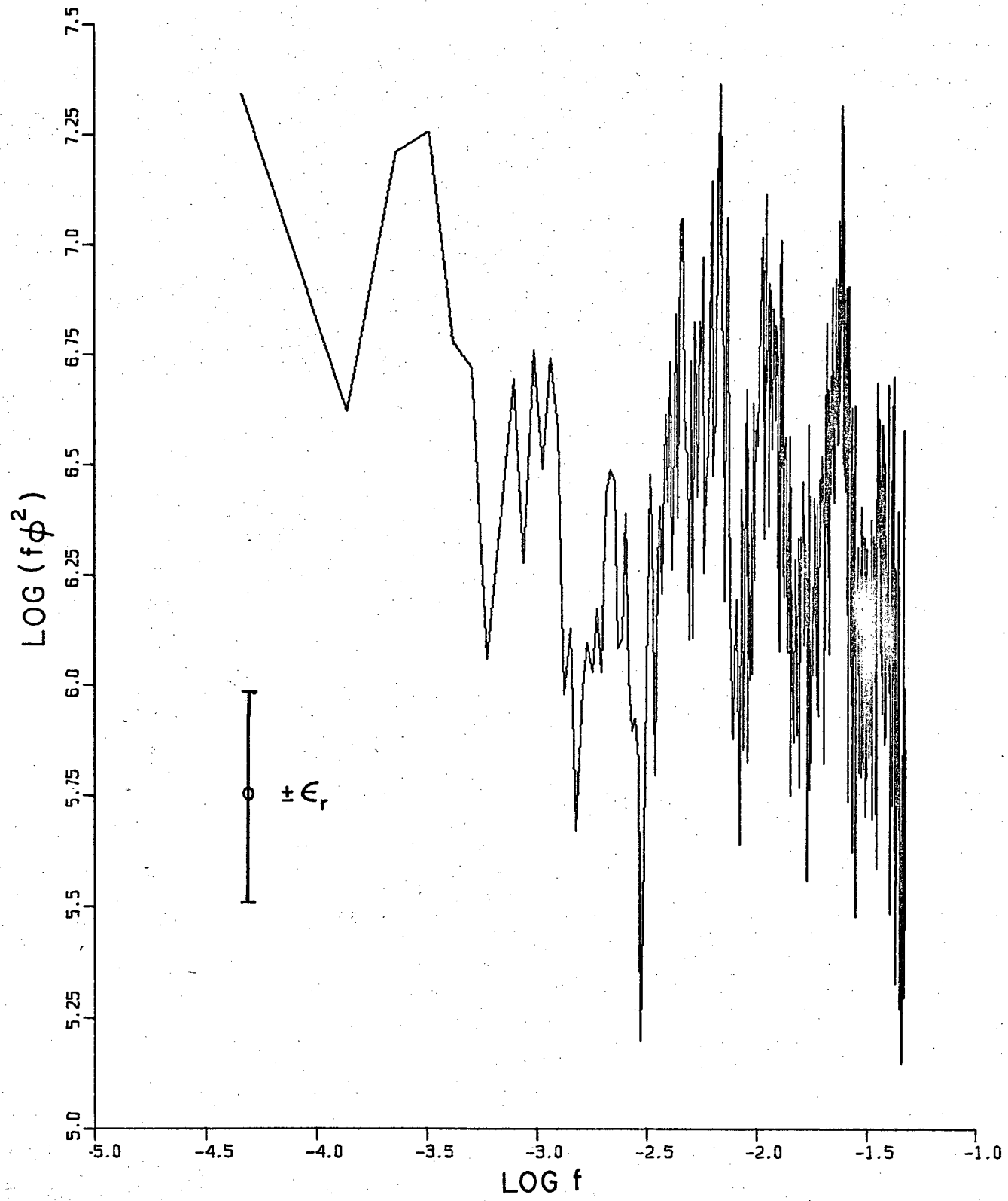

Fig. 2.13 The power spectrum for the polynomial - corrected time series in Fig. 2.10, smoothed over 4 points.

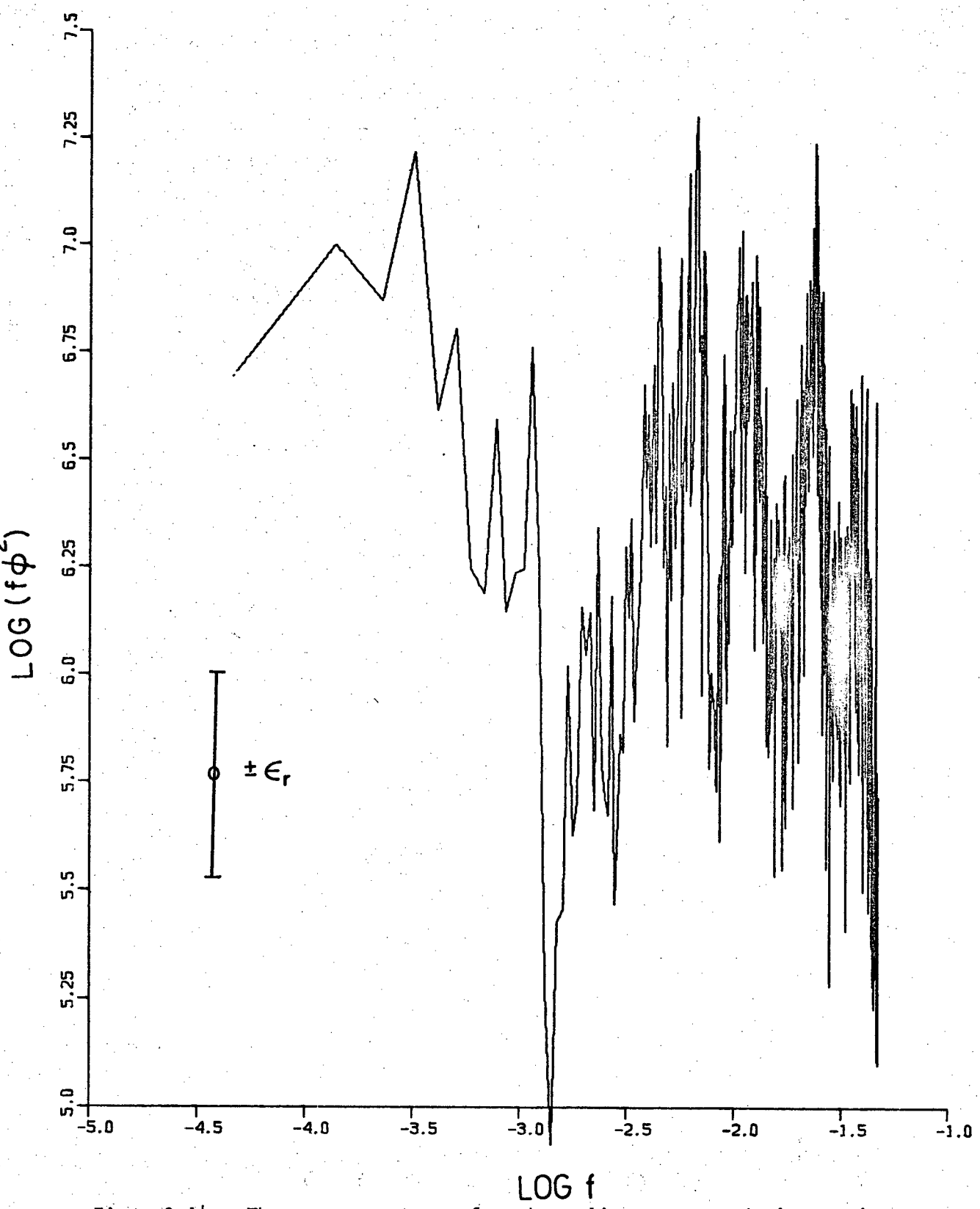

Fig. 2.14 The power spectrum for the spline-corrected time series in Fig. 2.12, smoothed over 4 points.

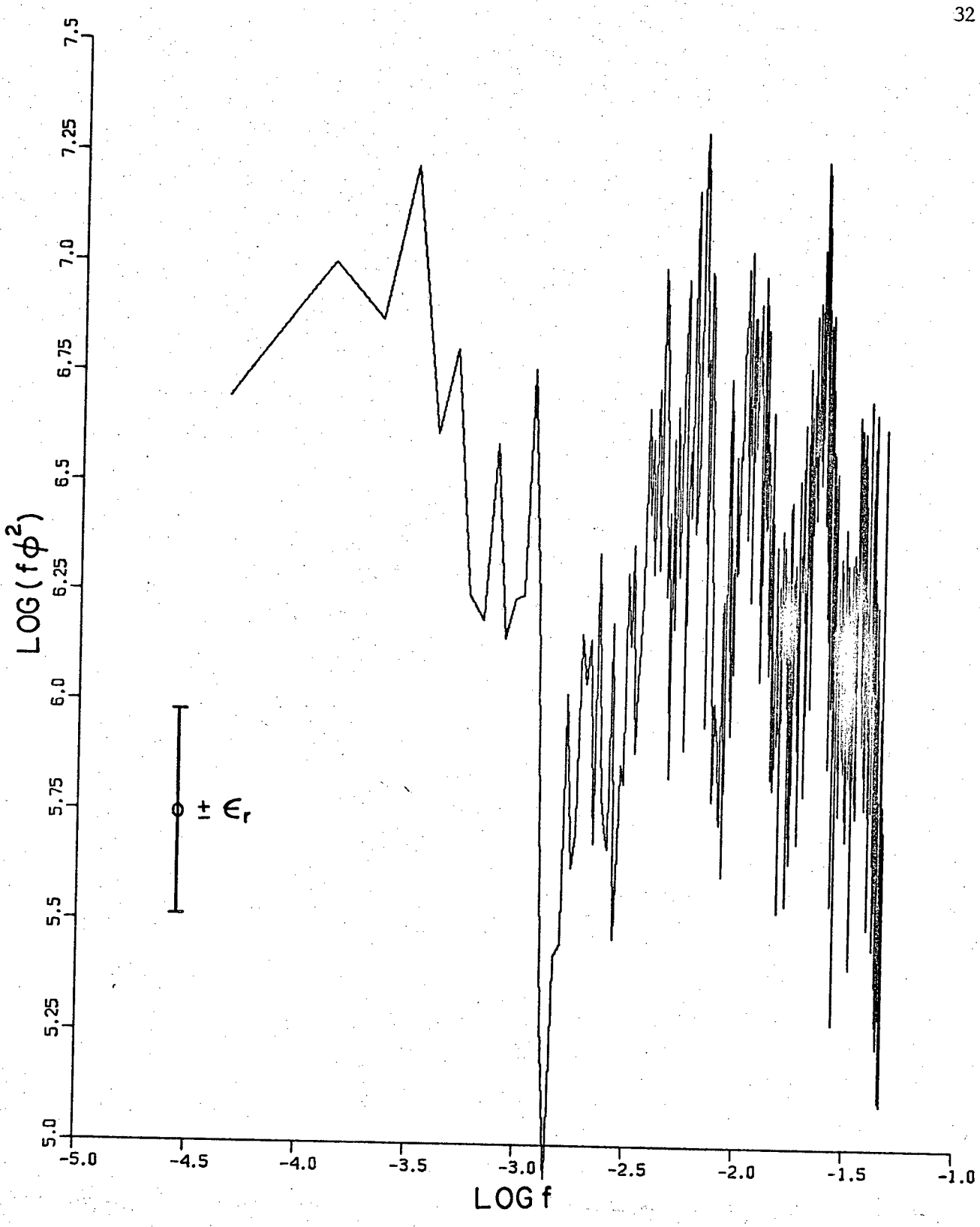

Fig. 2.15 The power spectrum for the spline - polynomialcorrected time series in Fig. 2.13, smoothed over44 points.

$$\varepsilon_r = \frac{\sigma[\hat{\phi}_{xx}(f)]}{\phi_x(f)} = \sqrt{\frac{2}{n}} \qquad \hat{\phi} = \text{computed value} \quad \phi = \text{real value} \tag{2.4}$$

where n is the number of degrees of freedom. Since each Fourier coefficient consists of an amplitude and a phase, averaging over d values produces a result with 2d degrees of freedom, so that

$$n = 2d$$

However, the average of the spectral estimates overaan interval $(f_0 - \Delta f/2,\ f_0 + \Delta f/2)$ when assigned to the frequency f_0 may not truly represent the spectral value at f_0. It may be greater or smaller, depending upon the shape of the spectrum. Thus , while averaging will reduce the effect of random errors in the individual spectral estimates, it does introduce a bias error.

Nevertheless, averaging is necessary if the spectral estimates are to carry any significance at all. The spectra in Figs. 2.13 to 2.15 have been averaged as described above, and the standard errors plotted were computed from 2.4.

These operations of tidal correction and cubic fitting were also performed on the record from channel 2; the high resolution, high-frequency record. A spectrum (Fig. 2.16) was calculated for this record as well, in order to compare it with the channel 4 results. In this way, any aliasing effects from the partial filtering performed on channel 4 could be discovered.

c) Discussion of the Spectra

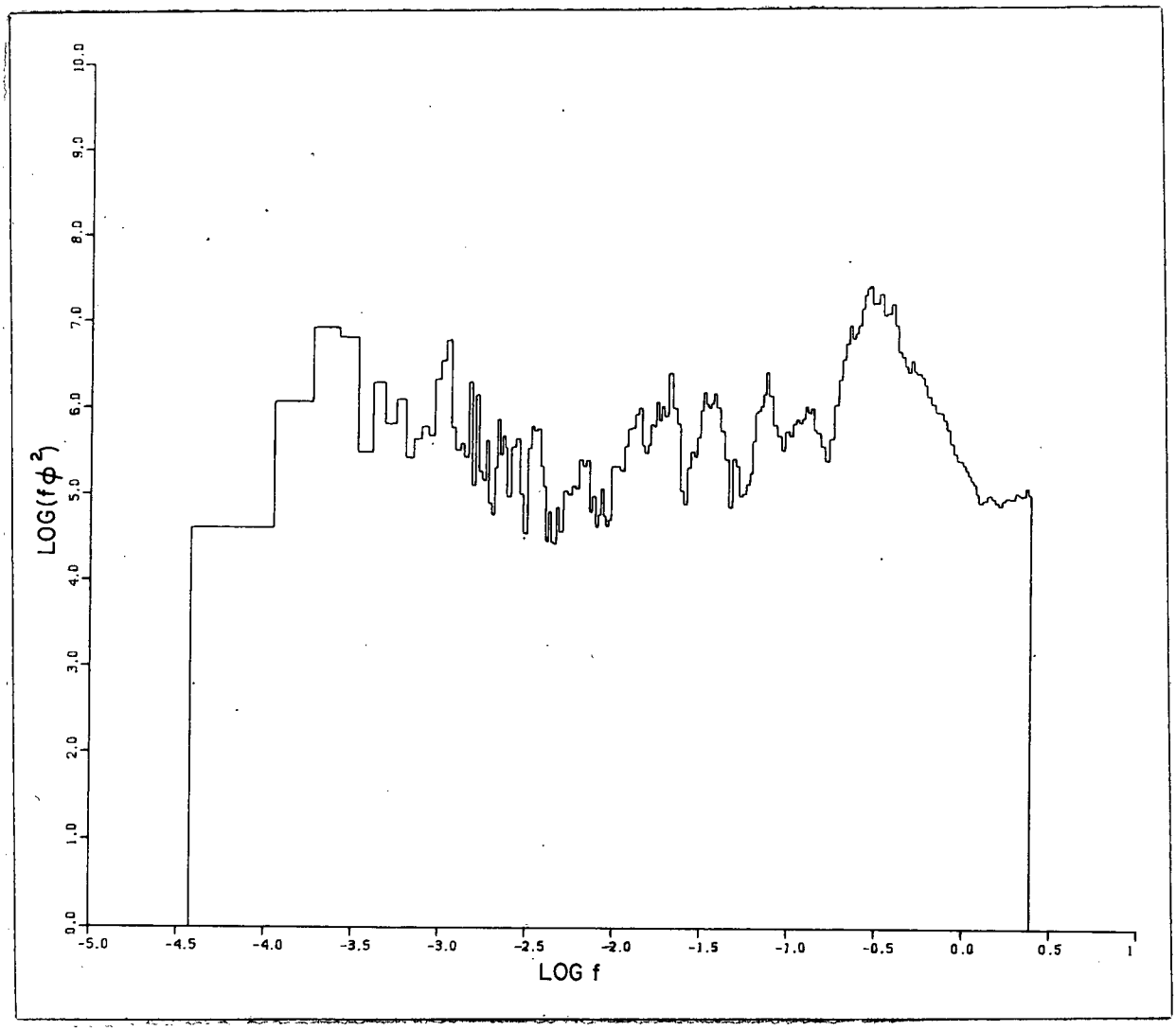

Fig. 2.16 The power spectrum for the polynomial - corrected time series from channel 2, logarithmically band averaged.

6) Discussion of the Spectra:

The spectrum shown in Fig. 2.14 is the four-point averaged spectrum of the spline-corrected time series in Fig. 2.12. Note the four prominent peaks in the low frequency portion of the spectrum. These have frequencies corresponding to periods of 55± 3 min., 38.5 ± 2 min., 21± 1 min. and 14.6 ± 6 min.

The peaks at 38.5 and 14.6 minutes correlate fairly well with the periods of motion observed in the government tide gauge traces. The other peaks do not. They do not, in fact, correlate with anything observed on the government gauge. There are two possible explanations for this. The first is that these do not correspond to real motions but are an artifact of some sort, introduced by the detrending procedures. If this were the case, then a spectrum produced by a different detrending procedure should alter these anomalous peaks.

With this in mind, examine Fig. 2.13 which is a spectrum of the same data, using a cubic polynomial fit instead of a spline fit. The same basic structure is still present, although not as clearly. The peak at ~ 15 min. period has split into two, although the two peaks are not really resolved. The peak at 38.5 min. appears now as no more than a shoulder on the 55 min. peak which has become much broader.

Fig. 2.15 shows the spectrum calculated from the spline corrected time series after it had again been fitted by the polynomial method. There

is no significant difference between this spectrum and the spectrum of the spline-fitted record. This is because the program choose a linear fit as best, and changed the time series only by a very small amount.

The spectrum of channel 2 shown in Fig. 2.16 was computed in order to check on possible aliasing done on Channel 4 of the instrument. Although calculations showed that there should be no significant effects from this process on the low-frequency end of the spectrum, comparison with the unfiltered record serves as a valuable check. The sampling rate was sufficiently high to resolve completely the surface wave spectrum which may be seen centred about a frequency of 0.3 hz.

The structure of the low-frequency region shows the same peaks found in the filtered spectra. The frequencies and relative magnitudes are the same, which leads to the conclusion that the filter installed in the low sampling frequency circuit had adequately suppressed the aliasing effects.

Examination of these spectra resulting from the various detrending methods leads to the conclusion that while some portions of the anomalous low-frequency energy may be artifacts introduced by the detrending most of it must be real.

It is possible only to speculate on possible sources of

this energy. Some of it may just be spurious values remaining because of imperfect detrending. The rest may be a response to long waves of various sorts which impinge upon the entrance of the bay. A wide spectrum of frequencies is possible for edge waves along this coast (see chapter 3, section 2) and the bay will respond to some extent to all of them, although not in a resonant mode.

The data set I obtained did not contain a very strong example of the seiche and the possibility exists, therefore, that the response seen at other frequencies was simply the off-resonance response of the system to forcing at those frequencies.

Taken in conjunction with the government tide gauge records, the results presented here support values of 38.5±2 min. and 14.6±.6 min. for the first and second longitudinal seiche modes, although the error involved is rather large. The quoted errors are equal to one half the bandwidth over which the spectral values were averaged at those frequencies.

The difficulty identifying the seiche motions clearly in the spectrum terms from the nature of the seiche in Port Renfrew itself. As the government tide gauge record showed, it is of small amplitude, short duration and random occurrence. The signal usually remains coherent over only a few periods, and thus is always superimposed on a large tidal trend. The effect cannot be avoided by taking longer records to resolve the tide, since the seiche (if it occurs at all) will not occur throughout the full length of the record, but only for a relatively short time.

Because of the error effects explained above, an oscillation lasting only a few periods will unaviodably have a large error in the Fourier coefficients; thus an incoherent signal like the seiche cannot be defined precisely. The effects of the large tidal trend only aggravate the problem, as they can never be removed perfectly.

It does not appear, therefore, that a very much more precise measurement of the seiche is possible, although if one were to be lucky enough to encounter a stronger, more long-lasting manifestation than the one I found, some improvement could be possible. For example, a 15 cm oscillation, lasting 24 hours does occasionally occur (see Figs. 2.1 and 2.2). This might be expected to produce power spectral coefficients 10 times larger than those found here, with only half the error in frequency.

7) Damping Effects

Description of the seiche is not complete without an estimate of the damping of the motion as well as its period. In an open bay such as this the damping will arise from two sources; the first due to radiation of long wave energy from the mouth of the bay and the second from frictional damping in the shallow water of the bay itself. These two dissipative mechanisms combine to limit the amplitude of the seiche and to damp it out if the force driving it should cease to operate. It is not possible to

separate these two effects observationally, but their combined effect may be estimated by finding the Q of the bay.

Q may be estimated in two different ways from the data at hand. The first estimate is from the half power bandwidth Δf of the resonance peaks in the spectrum of the oscillations. In this case

$$Q = f_o/\Delta f$$

where f_o is the resonant frequency. Because of the unavoidable uncertainty in the spectra, it is only possible to obtain an order of magnitude estimate, which gives the following results.

Table IV

Q as a function of mode number.

Mode #	Q
1	8
2	7

These should be regarded as no more than order of magnitude results, meaning that Q for both modes is on the order of 10.

The other method to estimate Q is to use the decay time of the seiche once it has been excited. Q is related to the logarithmic decrement λ by

$$\lambda = \frac{\pi}{Q}$$

Inspection of the government tide gauge records in Fig. 2.1 and 2.2 reveals that the seiche decays in 4 or 5 periods, so

that

$$Q \approx 12 - 15$$

by this method, which agrees with the estimate derived from the bandwidth calculations.

CHAPTER 3

THEORY

3.1) Solution of the Long-Wave Equations for a Rectangular Bay with an Exponential Bottom.

Port San Juan is very close to rectangular in surface plan, and the bottom profile approximates an exponential very well. I shall therefore take as a model a rectangular bay of width 2w and length L , as sketched in Fig. 3.1. It shall have steep lateral walls, a sloping beach at the head (x = 0), and be open at the mouth (x = - L). The bottom depth will be allowed to vary with x as

$$h = h_o (1 - e^{cx}) , \qquad (3.1)$$

where the constants h_o and c are taken to match reality as closely as possible. The depth does not change with y, across the bay. Fig. 3.2 shows a comparison between the exponential bottom profile (3.1) and soundings from the chart of Port Renfrew. The agreement is quite good, with w = 1000 m, L = 6400 m, h_o = 16.97 m , c = 4.956 x 10^{-4} m^{-1} .

The analysis is performed under the following assumptions:

1) No rotation: the observed frequencies are sufficiently high (1-2 cycles/hour) that the Coriolis force is negligible.
2) Shallow water barotropic conditions, applicable to the propagation of long waves, are used throughout.
3) Linearized equations are used, adequate for small amplitude seiches.

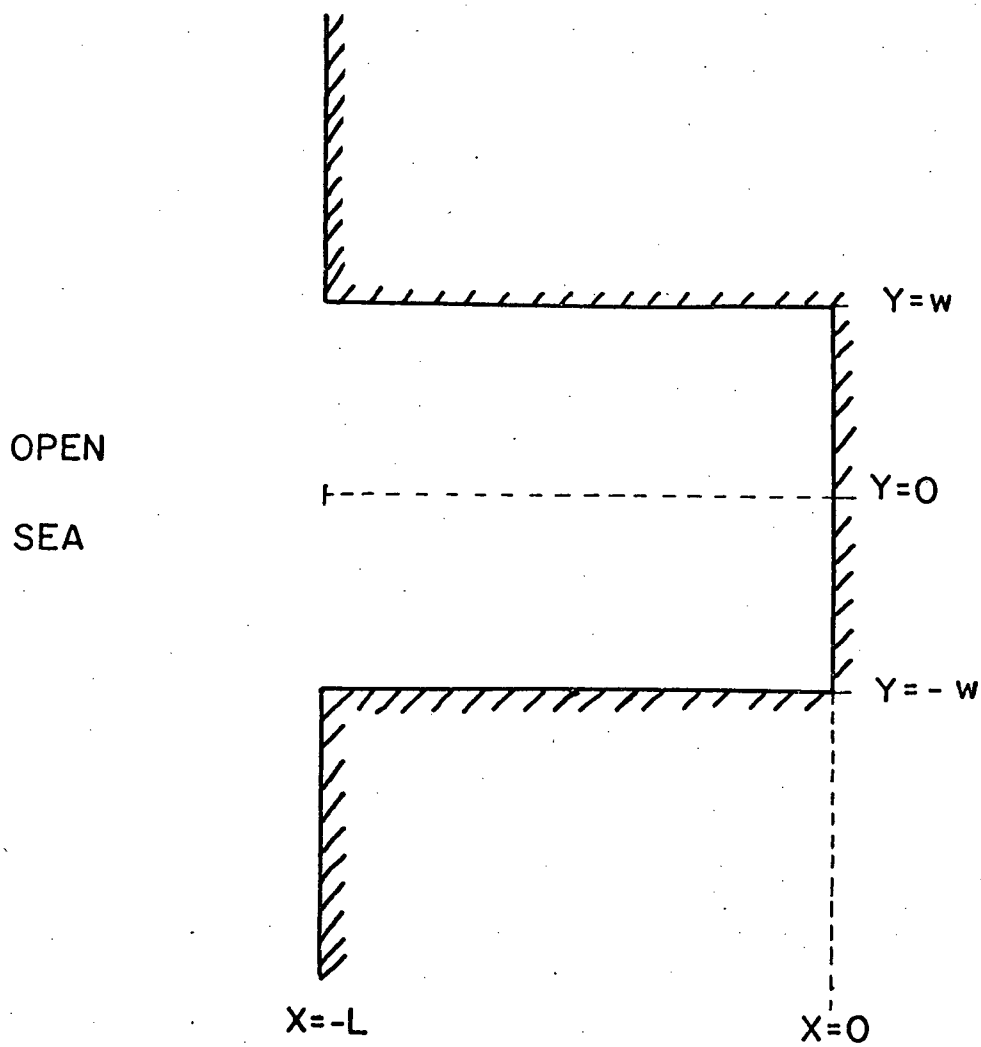

Fig. 3.1 The coordinate axes and the assumed geometry of Port San Juan for theory: L=6400m, w=1000m, h_o =16.97m, C=4.95596 x 10^{-4} $\frac{m}{s}$ = 1.

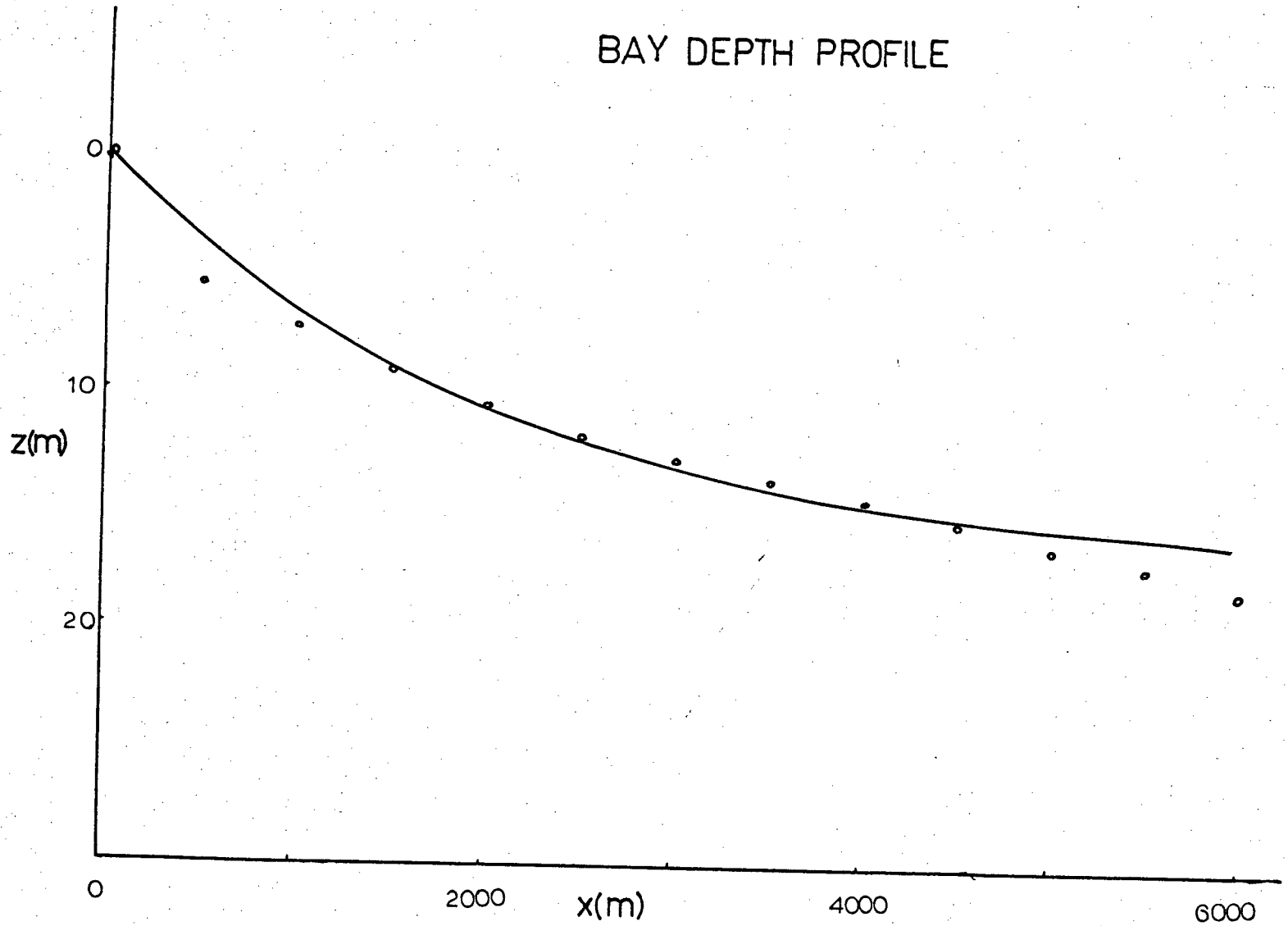

Fig. 3.2 A comparison of the theoretical and actual bottom profiles for Port San Juan. The solid line is the fitted theoretical curve; the open circles are soundings taken from the chart.

4) The depth depends on x only, as per (3.1).

Starting with the usual long-wave equations, with η the surface displacement from mean water level, u the current in the x-direction, and v the current in the y-direction:

$$\begin{aligned} \frac{\partial u}{\partial t} + g\frac{\partial \eta}{\partial x} &= 0 , \\ \frac{\partial v}{\partial t} + g\frac{\partial \eta}{\partial y} &= 0 , \\ \frac{\partial (hu)}{\partial x} + h\frac{\partial v}{\partial y} + \frac{\partial \eta}{\partial t} &= 0 . \end{aligned} \qquad (3.2)$$

The velocity components u and v are eliminated from the above to yield an equation for η alone:

$$\frac{\partial^2 \eta}{\partial t^2} - gh\left(\frac{\partial^2 \eta}{\partial x^2} + \frac{\partial^2 \eta}{\partial y^2}\right) - g\frac{dh}{dx}\frac{\partial \eta}{\partial x} = 0 . \qquad (3.3)$$

Let us look for harmonic solutions of the form

$$\eta(x,y;t) = F(x,y)\, e^{i\nu t} .$$

Substitution into (3.3) gives

$$\nabla^2 F + \frac{h_x}{h} F_x + \frac{\nu^2}{gh} F = 0 . \qquad (3.4)$$

Note the presence of the F_x term, due to the inclusion of bottom topography. With the specific bottom profile (3.1), the coefficient of F_x has the following form:

$$\frac{h_x}{h} = -\frac{c\, e^{cx}}{1 - e^{cx}} .$$

Let's write $F(x,y) = X(x)\,Y(y)$; then (3.4) takes the following form,

where primes indicate differentiation with respect to the relevant arguments:

$$\frac{X''}{X} + \frac{Y''}{Y} - \frac{c\, e^{cx}}{1 - e^{cx}} \frac{X'}{X} + \frac{\nu^2}{gh_o(1-e^{cx})} = 0 . \quad (3.5)$$

This equation must be solved in the bay subject to the relevant boundary conditions.

At the sides, $y = \pm w$ there are steep walls, through which no flow may pass; therefore,

$$v = 0 \text{ , i.e. } F_y = 0 \text{ at } y = \pm w. \quad \text{(B.C.I)}$$

At the head of the bay ($x = 0$) there is a sloping beach, so that the depth $h \to 0$ at $x = 0$. (This produces a regular singular point at $x = 0$ in the equation for η.) The wave runs up some distance on the beach: the appropriate boundary condition at $x = 0$ is then merely that both η and u be finite:

$$F \text{ , } F_x \text{ finite at } x = 0 . \quad \text{(B.C.II)}$$

At the mouth, $x = -L$, both current and pressure must be continuous, which means that both $\eta(-L)$ and $u(-L)$ must match the outside solution. This will be dealt with later, after the solution for the exciting wave has been found.

Equation (3.5) is separable; the solution for Y subject to (B.C.I) may easily be found to be

$$Y(y) = A \cos\left[\frac{n\pi}{2w} (y-w)\right] , \quad (3.6)$$

with $n = 0, \pm 1, \pm 2, \ldots$ Substituting for (3.6) into (3.5), the X dependence is now given by

$$X'' - \frac{c\, e^{cx}}{1-e^{cx}} X' + \left[\frac{\nu^2}{gh_o(1-e^{cx})} - \frac{n^2\pi^2}{4w^2} \right] X = 0 . \quad (3.7)$$

Let us introduce the new variables

$$\kappa = n\pi/2wc \quad ; \qquad \sigma^2 = \nu^2/gh_o c^2 \; ;$$

$$s = e^{cx} \quad ; \qquad X(x) = G(s) \quad .$$

Equation (3.7) for X(x) then becomes for G(s):

$$s^2(1-s)G'' + s(1-2s)G' + \left[\sigma^2 - \kappa^2(1-s)\right] G = 0 . \quad (3.8)$$

This equation has regular singular points at $s = 0$ ($x = -\infty$), and $s = 1$ ($x = 0$, the head of the bay); it is an equation of the general form

$$s^2(1-s)G'' + s(a_1 + b_1 s)G' + (a_2 + b_2 s)G = 0,$$

with

$$a_1 = 1 , \qquad a_2 = \sigma^2 - \kappa^2 ,$$

$$b_1 = -2 , \qquad b_2 = \kappa^2 .$$

Now let $G = s^k u$, where

$$k^2 + k(a_1 - 1) + a_2 = 0,$$

or $k^2 = \kappa^2 - \sigma^2$.

Replacing G by u, (3.8) becomes

$$s(1-s)u'' + (a - bs)u' + cu = 0, \quad (3.9)$$

with

$$a = 2k + a_1 = 1 \pm 2(\kappa^2 - \sigma^2)^{1/2} ,$$

$$b = 2k - b_1 = 2\left[1 \pm (\kappa^2 - \sigma^2)^{1/2} \right] ,$$

$$c = b^2 + (1+b_1)k - k^2$$

$$= \sigma^2 \mp (\kappa^2 - \sigma^2)^{1/2} .$$

With these substitutions, (3.9) takes the form

$$s(1-s)u'' + [1 \pm 2\sqrt{\kappa^2-\sigma^2} - 2(1 \pm \sqrt{\kappa^2-\sigma^2})s]u' + (\sigma^2 \mp \sqrt{\kappa^2-\sigma^2})u = 0. \qquad (3.10)$$

This is a form of Gauss' Hypergeometric Equation (Erdelyi et al., 1953):

$$s(1-s)u'' + [c-(1+a+b)s]u' - abu = 0,$$

with

$$a = \frac{1}{2}[1 + 2\sqrt{\kappa^2-\sigma^2} \pm \sqrt{1+4\kappa^2}],$$

$$b = \frac{1}{2}[1 + 2\sqrt{\kappa^2-\sigma^2} \mp \sqrt{1+4\kappa^2}],$$

$$c = 1 + 2\sqrt{\kappa^2-\sigma^2},$$

and where the positive root has been chosen for $\sqrt{\kappa^2-\sigma^2}$. I shall also choose the positive root for $\sqrt{1+4\kappa^2}$, since the other sign merely interchanges a and b and the equation is symmetric in those quantities.

Equation (3.10) is that special form of Gauss' Hypergeometric Equation in which a,b,c, satisfy the relation

$$c - a - b = -q; \quad q = 0,1,2,.....$$

In this case, q = 0. For this special form, the general solution consists of a sum of two linearly independent solutions expanded about the regular singular point at x = 0 (Murphy, 1960); these two solutions are

$$y_1 = {}_2F_1(a,b;1;z)$$

$$y_2 = y_1 \ln(z) + Y(a,b;1;z),$$

where ${}_2F_1$ has the series expansion

$$ {}_2F_1(a,b;c;z) = \frac{\Gamma(c)}{\Gamma(a)\Gamma(b)} \sum_{j=0}^{\infty} \frac{\Gamma(a+j)\Gamma(b+j)}{\Gamma(c+j)\ j!} z^j , $$

and the exact form for Y need not be written, as the second solution will be rejected.

The condition (B.C.II) requires that the solution be finite at the head of the bay. The head of the bay (x=0) corresponds to $z = 1-e^0 = 0$. The second solution, y_2, becomes negatively infinite there and must therefore be discarded.

The general solution for the x-dependence (in the original variables) is therefore

$$ X(x) = A \exp[c\sqrt{\kappa^2-\sigma^2}\, x] \sum_{j=0}^{\infty} \frac{\Gamma(a+j)\Gamma(b+j)}{\Gamma(a)\Gamma(b)\ j!\ j!} (1 - e^{cx})^j . \qquad (3.11) $$

The constants $\sqrt{\kappa^2-\sigma^2}$, a, and b are in general complex. X(x) will be complex and oscillatory in character if $\kappa^2<\sigma^2$; this is certainly the case when there is no cross-channel variation (n=0).

The complete solution for the amplitude inside the bay is then

$$ \eta_n(x,y;t) \doteq \text{Real}\left\{A_n \exp[c\sqrt{\kappa^2-\sigma^2}\, x]\ {}_2F_1(a,b;1;1-e^{cx})\right\} \cos[n\pi(y-w)/2w]\cos\nu t, \qquad (3.12) $$

for the n^{th} cross-channel mode.

This solution must be matched to the outside solution, which drives that inside the bay.

3.2) The Outside Edge Wave.

To calculate the form of an edge wave travelling along the coast outside Port San Juan, I shall follow the treatment given by Ball (1967).

The shelf profile off Port San Juan is a good fit to an exponential of the form

$$h = h_o(1 - e^{bx}) , \qquad (3.13)$$

with

$$h_o = 112.22 \text{ m} ,$$
$$b = -3.545 \times 10^{-4} \text{ m}^{-1}.$$

Fig. 3.3 shows a comparison between the fitted function and soundings taken from the hydrographic chart.

Let now x = 0 along a straight coastline, stretching to $y = \pm \infty$ as in Fig. 3.4.

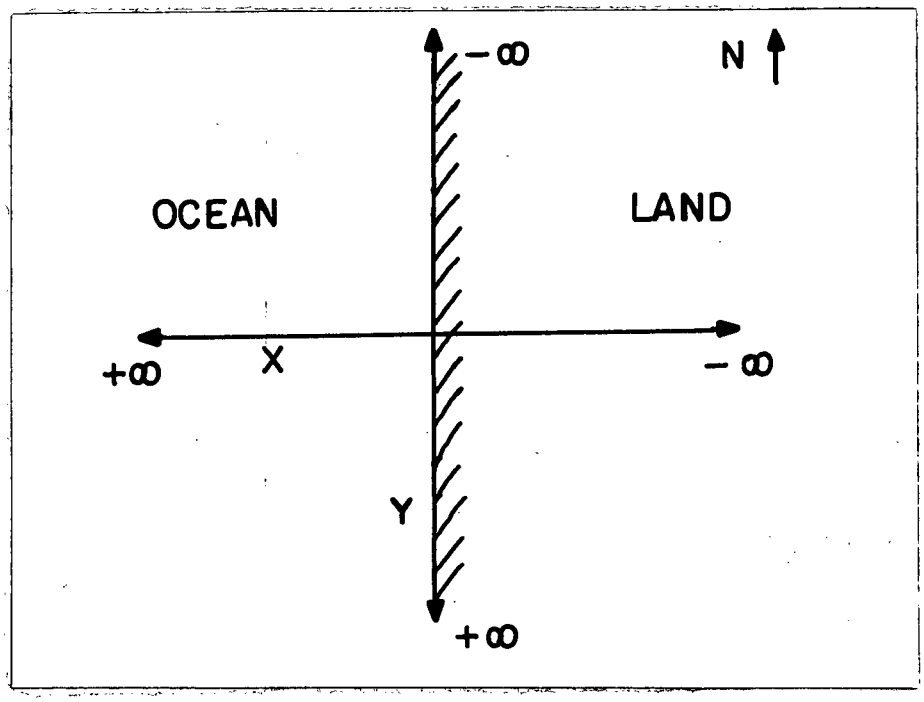

Fig. 3.4 The coordinate axes for the outside wave calculations.

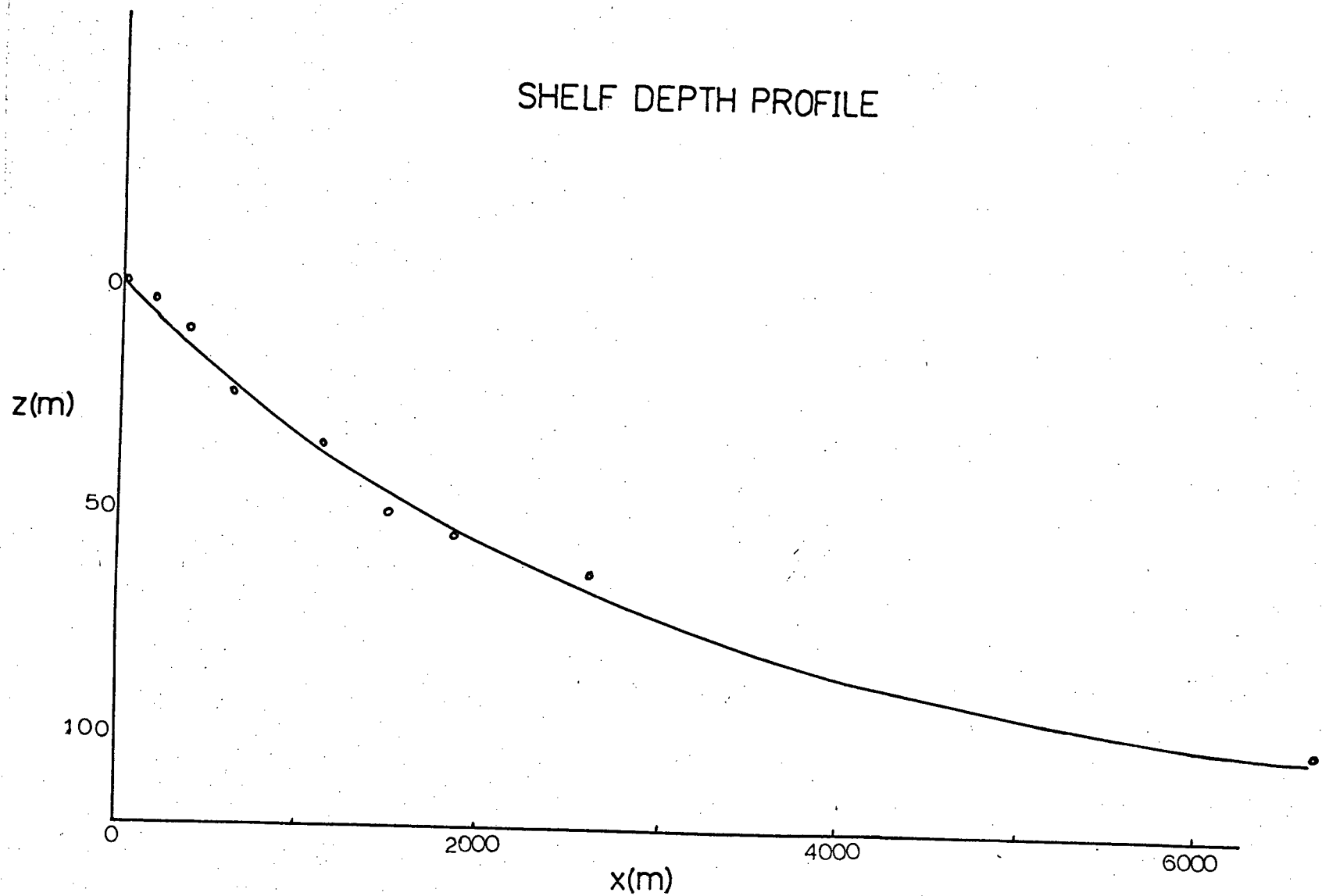

Fig. 3.3 A comparison of theoretical and actual bottom profiles for the shelf off Port San Juan. The solid line is the assumed profile; the circles are soundings taken from the chart.

Starting from the equation for the surface elevation η (3.3), we look for travelling wave solutions along the coast, of the form

$$\eta_o(x;y;t) = F(x) \exp[i(\nu t - my)].$$

Under the same assumptions used for the analysis inside the bay, and now using the new variables

$$s = e^{bx}, \qquad \sigma^2 = \nu^2/gh_o b^2,$$
$$k = m/c, \qquad F(x) = G(s)$$

These transformations lead to the equation

$$s^2(1-s)G'' + s(1-2s)G' + [\sigma^2 - k^2(1-s)]\,G = 0 \qquad (3.14)$$

for the surface elevation, a form identical to that found in the previous analysis (3.8).

Looking for a series solution about $x = -\infty$, subject to the boundary conditions that F and F' must both be finite at x= 0, and F→0 as $x \to -\infty$, we first define

$$p^2 = k^2 - \sigma^2 . \qquad (3.15)$$

The requirement that F tend to zero as x tends to minus infinity demands that the series for F terminate after a finite number of terms, which means that

$$k^2 = (p+n)(p+n+1) , \qquad (3.16)$$

where n is an integer. This gives for G(s) the solution

$$G(s) = A\, s^p\, {}_2F_1(-n, n+2p+1; 2p+1; s) . \qquad (3.17)$$

(The boundary condition at the coast allows us to discard the second solution, which has a logarithmic singularity there).

There are therefore a whole hierarchy of modes possible, corresponding to different values of n. The zeroth-order modes are the most easily stimulated (Ball, 1967), and therefore the most likely to be present. I shall accordingly take the outside exciting wave to be a zeroth-order edge wave. In that case, $n = 0$, and (3.14) and (3.15) reduce to

$$p^2 = k^2 - \sigma^2 ,$$
$$k^2 = p^2 + p , \qquad (3.18)$$

which gives, eliminating p,

$$\sigma^2 = \frac{1}{2} [-1 \pm \sqrt{1 + 4k^2}] . \qquad (3.19)$$

Choosing the positive root gives real travelling wave solutions. We therefore use

$$\sigma^2 = \frac{1}{2} [\sqrt{1 + 4k^2} - 1]. \qquad (3.19a)$$

Substituting for periods comparable to those of the seiches observed in the bay into (3.19a) yields zeroth-mode wavelengths as given in Table 3.1. For these short periods, the form of the edge waves is controlled by the topography, and not by the rotation; these waves can therefore travel at equal speeds in either direction along the coast.

Period (min.)	Wavelength (km)
60	119.4
30	59.7
15	29.8

Table 3 V. The wavelength of zeroth-mode edge waves for a few selected periods.

The zeroth order mode has the form

$$\eta(x,y;t) = A_o e^{pbx}\ {}_2F_1(0,2p+1;2p+1;e^{bx})\ e^{i(\nu t - my)} \quad . \tag{3.20}$$

But(Abramowitz and Stegun, 1970, p556),

$${}_2F_1(a,b;b;z) = (1-z)^{-a}.$$

Here, $a = 0$, and the outside wave reduces to

$$\eta_o(x,y;t) = A_o \exp(\sigma^2 bx)\ e^{i(\nu t - my)} \quad . \tag{3.21}$$

At the coast, we find for the real part of the outside wave displacement:

$$\eta_o(0,y;t) = A_o \cos(\nu t - my). \tag{3.22}$$

3.3) Matching the solutions.

In order to find the complete motion inside the bay, we must now match the free inside solutions with the outside forcing wave at the mouth of the bay. The necessary boundary conditions are continuity of pressure and current across the mouth of the bay. Under the assumptions made at the beginning of the chapter, these requirements are satisfied by the continuity of current and surface elevation across the mouth. This balance cannot however be expressed simply as an equality between the inside free wave and the outside wave; this would overdetermine the system. The presence of the open mouth of the bay means that the induced oscillation inside will radiate energy in the form of long waves out into the open sea. The appropriate matching is therefore between the outside, inside and scattered waves, as given by

$$\eta_i(-L) = \eta_o(0) + \eta_s(0) \ ,$$
$$u_i(-L) = u_o(0) + u_s(0) \ . \qquad (3.23)$$

The meaning of the subscripts should be clear from what has been explained above. Different arguments apply to the inside and outside coordinate systems, as they have been defined differently (see Fig. 3.1 and Fig. 3.4). The equations (3.23) must be solved for the unknown amplitude coefficients A_n of the inside solution in order to find the resonant response.

It is now necessary to find a form for the scattered wave, in in terms of the existing elevation at the mouth.

Matching must be done for each of the hierarchy of cross-channel modes. In order to do this correctly, the outside exciting wave must be decomposed into an eigenfunction expansion in terms of the cross-channel modes of the inside system. From (3.6), the inside cross-channel eigenfunctions are

$$\phi_n = \cos[n\pi(y-w)/2w] \ . \qquad (3.24)$$

Taking the real part of (3.21) as the outside wave, it is necessary to express (3.22) in the form

$$\eta_o = \sum_n \alpha_n \phi_n \cos\nu t + \sum_n \beta_n \phi_n \sin\nu t \ . \qquad (3.25)$$

Inside the bay, only the eigenfunctions (3.24) exist, and therefore, η_o must be continued as an even function in $[-w,3w]$, in order to perform the expansion correctly. The result is the same as far as the inside response is concerned.

Transform variables by letting $\xi = y - w$. In the equation for η_o simply replace y by ξ to simplify the integrations. This merely introduces a change of phase in η_0, which was arbitrary in the first place.

Then

$$\alpha_n = \frac{1}{2w} \int_{-2w}^{2w} A_{out}\, e^{-pbL} \cos(m\xi) \cos(n\pi\xi/2w)\, d\xi \,,$$

$$\beta_n = \frac{1}{2w} \int_{-2w}^{2w} A_{out}\, e^{-pbL} \sin(m\xi) \cos(n\pi\xi/2w)\, d\xi \,. \qquad (3.26)$$

Evaluation of these integrals yields

$$\alpha_n = \frac{m\, A_{out}\, e^{-pbL} \sin(2mw) \cos(n\pi)}{w\, [\, m^2 - n^2\pi^2/4w^2 \,]} \,,$$

$$\beta_n = \frac{m\, A_{out}\, e^{-pbL} [\, \cos(2mw)\cos(n\pi) - 1]}{w\, [\, m^2 - n^2\pi^2/4w^2 \,]} \,. \qquad (3.27)$$

These expressions may then be used to evaluate the outside elevation in terms of the cross channel modes of the bay.

Reference to Table 3.1 shows that for periods comparable to those observed, the wavelengh of η_{out} is very much longer than the 2Km entrance width of the bay. In this case we may

neglect the excitation of the higher modes and be concerned only with the case where n=0: the amplitude of the exciting wave is then taken as constant across the mouth. (There is a change in phase, due to the travelling nature of the wave, which will cause the modes inside the bay to be forced with two different phases - the usual cos νt term and another in sin νt; this is of no consequence, however, in computing the resonant response frequencies).

The problem to be dealt with now is how best to account for the scattering of waves from the entrance of the bay when attempting to match the solutions across the entrance. In order to do this I shall follow the approximate equivalent - circuit analysis method of Miles (1971) as modified by Garrett (1975).

In this formulation the edge wave produces an elevation η_0 at the mouth of the bay; the surface of the bay being taken as being at rest. The discrepancy in elevation at the mouth of the bay then produces a mass flux F through the mouth of the bay, in order to balance the pressure difference at the mouth. This in turn forces a response η_i inside the bay, and scatters waves out into the open ocean. The relationships between these various quantities are analogous to those in an electrical circuit, and may be treated correspondingly. I shall treat only the case where the cross-channel mode number is zero, and leave the problem of the higher-order cross-channel modes until later (see appendix A).

I shall follow the method of Garrett, and first define the impedance of the bay itself and that of the ocean outside. The elevation discrepancy at the mouth of the bay induces a flux F through the mouth of the bay. Let a point source of transport in the mouth $h \underset{\sim}{u} \cdot \underset{\sim}{n} = \delta(s-\sigma)$ produce the responses $K_B(s,\sigma)$ and $K_o(s,\sigma)$ on the bay and open ocean sides respectively. Then, equations (3.23) require that

$$\int_M K_B(s,\sigma)\, F(\sigma)\, d\sigma = \eta_o(s) - \int_M K_o(s,\sigma)\, F(\sigma)\, d\sigma \quad , \quad (3.28)$$

which defines an integral equation for $F(\sigma)$.

If we assume that there are no cross-channel modes and that the bay mouth is small with respect to the wavelength of free waves, η_0 and η_i are independent of $\hat{s}$ (distance across the mouth) and we can define

$$F(\sigma) = I\, f(\sigma) \quad , \quad (3.29)$$

where $\int_M f(\sigma)\, d\sigma = 1$, and I is the mass flux through the mouth, Then if we define an equivalent exciting voltage V_o by

$$V_o = \int_M \eta_o(s)\, f(s)\, ds \quad , \quad (3.30)$$

(3.28) becomes

$$Z_B I = V_o - Z_o I, \quad (3.31)$$

where the impedances Z_B and Z_o are defined by

$$Z_B = \int_M \int_M K_B(s,\sigma)\, f(s) f(\sigma)\, d\sigma ds \quad ,$$

$$Z_o = \int_M \int_M K_o(s,\sigma)\, f(s) f(\sigma)\, d\sigma ds \quad . \tag{3.32}$$

These impedances define the relation between the elevation of the surface at the mouth and the corresponding flux through it. They are stationary with respect to small changes of f(s) about the exact solution (Miles 1971) and therefore may be approximated quite well by trial solutions. The solution of (3.31) gives the flux through the mouth

$$I = \frac{V_G}{Z_o + Z_B} \quad , \tag{3.33}$$

and the corresponding elevation

$$V_m = \frac{Z_B V_o}{Z_o + Z_B} \quad , \tag{3.34}$$

which is not very different from V_o if $Z_B >> Z_o$, a condition which can be obtained if there is either a large change of depth from the bay to the deep ocean (in this case a factor of ~ 7) and the bay is relatively small (as this one is).

Since the solutions for the free waves inside the bay are known, it is a simple matter to find Z_B since

$$Z_B = \frac{V_B}{I} = \eta_i(-L)/[2wh_m u_i(-L)] , \qquad (3.35)$$

where V_B is defined as in (3.30), and h_m is the depth at the mouth. Using (3.2) for $u_i(x)$ and (3.11) for $X(x)$ gives

$$u_i(x) = \frac{-ig}{\nu} \text{Real}[X'(x)] , \qquad (3.36)$$

where

$$X'(x) = A \exp[c\sqrt{\kappa^2-\sigma^2}\, x] \left[(c\sqrt{\kappa^2-\sigma^2})\, {}_2F_1(a,b;1;1-e^{cx}) \right.$$
$$\left. -abc\, e^{cx}\, {}_2F_1(a+1,b+1;2;1-e^{cx}) \right] ,$$

using the form given by Abramowitz and Stegun (1970) for the derivative of ${}_2F_1(a,b;1;z)$. In this case, the bay impedance Z_B becomes

$$Z_B = i\nu \text{ Real} \left\{ \exp[-c\sqrt{\kappa^2\ \sigma^2}\ L]\ {}_2F_1(a,b;1;1-e^{-cL}) \right\} \cdot$$
$$\left\{ 2wh_o(1-e^{-cL}) \text{ Real} \left[\exp[-c\sqrt{\kappa^2\ \sigma^2}\ L] \left(c\sqrt{\kappa^2\ \sigma^2}\ {}_2F_1(a,b;1;1-e^{-cL}) \right.\right.\right.$$
$$\left.\left.\left. - abc\, e^{-cL}\, {}_2F_1(a+1,b+1;2;1-e^{-cL}) \right) \right] \right\}^{-1} . \qquad (3.37)$$

In order to solve the problem completely, an expression for the impedance of the outside ocean to scattered waves must be found.

Given a unit current impulse in the mouth of the bay, the outgoing waves produced in an ocean of uniform depth are given (Miles, 1971; Buchwald, 1971) by the integral of a Green's function which is a cylindrical Hankel function. At the bay mouth itself (x = - L), this takes the form

$$K_o(y,\eta) = \frac{\nu}{2gh_{out}} H_o^{(2)}(k_o|y-\eta|) , \qquad (3.38)$$

with $k_o = \nu/\sqrt{gh_{out}}$, since we are dealing with frequencies where f becomes negligible.

The depth h_{out} appearing in (3.38) is the asymptotic value of the actual offshore depth. The assumption has been made that the effect of the sloping bottom is not too great, and that the Green's function (3.38) appropiate for a flat-bottomed, frictionless ocean may be used. There does not exist in the literature, to my knowledge, a Green's function appropriate for a sloping bottom. See appendix B for further comments on this problem.

Using (3.38) the outside impedance (from 3.32) is given by

$$Z_o = \frac{\nu}{2gh_o 4w^2} \int_{-w}^{w}\int_{-w}^{w} H_o^{(2)}(k_o|y-\eta|)\,d\eta dy \qquad (3.39)$$

The function f(s) has been simply taken as $\frac{1}{2w}$, since in the case of no cross-channel variation this is very nearly correct. $2k_o w$ is of the order of 1/30 and therefore the asymptotic form of $H_o^{(2)}(z)$ for small z may be used (Abramowitz & Stegun, 1970):

$$H_o^{(2)}(z) \sim 1 - \frac{2i}{\pi}[\ln(z/2) + \gamma],$$

where $\gamma = 0.57721...$ is Euler's constant.

Evaluation of the integral gives

$$Z_o = \frac{\nu}{2gh_{out}} \left\{ 1 - \frac{2i}{\pi}\left[\ln[\nu w/\sqrt{gh_o}] + \gamma - 3/2 \right] \right\} . \qquad (3.40)$$

V_o must be evaluated next; from (3.22) and (3.20),

$$V_o = \int_{-w}^{w} \frac{A_{out}}{2w} \cos[\nu t - my]\, dy \,, \qquad (3.41)$$

$$= \frac{A_{out} \cos(\nu t) \sin(mw)}{wm} \,.$$

The flux through the mouth given by (3.32) takes the form

$$I = \frac{V_o}{Z_o + Z_B} = \frac{A_{out} \cos(\nu t) \sin(mw)}{Z_o + Z_B} \,. \qquad (3.42)$$

Resonance will occur when there is a minimum in $| Z_o + Z_B |$. This produces a large flux through the mouth, and a correspondingly large surface elevation at the head of the bay.

Because of the complicated nature of the functions involved, it is not possible to solve analytically for the minima of $|Z_o + Z_B|$. The hypergeometric functions are not tabulated and therefore must be evaluated from the series expansion in (3.11). A Fortran program was written to sum up terms of the series. Convergence to within 1 part in 10^6 was found after 300 terms were added. In order to find the resonant frequencies and the shape of the response curve for the bay, a program was written to evaluate I as a function of ν and also to calculate η vs ν at the position corresponding to the wharf where the measurements were taken. The value of η at the wharf is given by

$$\eta(x_w) = \frac{V_m}{\eta(-L)} \text{ Real } \left\{ \exp\left[-c\sqrt{\kappa^2 - \sigma^2}\, x_w\right] {}_2F_1(a,b;1;1-e^{-cx_w}) \right\} , \quad (3.43)$$

where $x_w = -2000$ m is the position of the wharf, and V_m is given by (3.34).

Fig. 3.5 shows I as a function of frequency. The forcing function was as in (3.41), with $A_{out} = 0.5$ cm. The graph shows the magnitude of the flux through the mouth as a function of frequency. There are two peaks; the first at a frequency of 3.02×10^{-3} Hz corresponding to a period of 34.67 minutes; the second at a frequency of 7.78×10^{-3} Hz corresponding to a period of 13.46 min. The resonance peaks are of finite width and height due to the effect of the radiation of waves from the mouth of the bay. This effect is due to the real part of Z_o, which limits the value of $V_o/[Z_o+Z_B]$, since Z_B is purely imaginary. Reference to (3.40) demonstrates that Real(Z_o), and hence the radiative damping, increases linearly with ν. This effect is recognizable in the decreasing amplitude of the resonance peaks as ν increases in Fig. 3.5. The value of the radiative Q,

$$Q = f_o / \Delta f$$

in each case is as follows in the computed response:

First mode: Q = 21.57,

Second mode : Q = 32.42 .

Fig. 3.6 shows the surface amplitude and phase (dotted line) relative to the exciting current at the position of the wharf. The second resonance peak appears very much lower than the first because the wharf

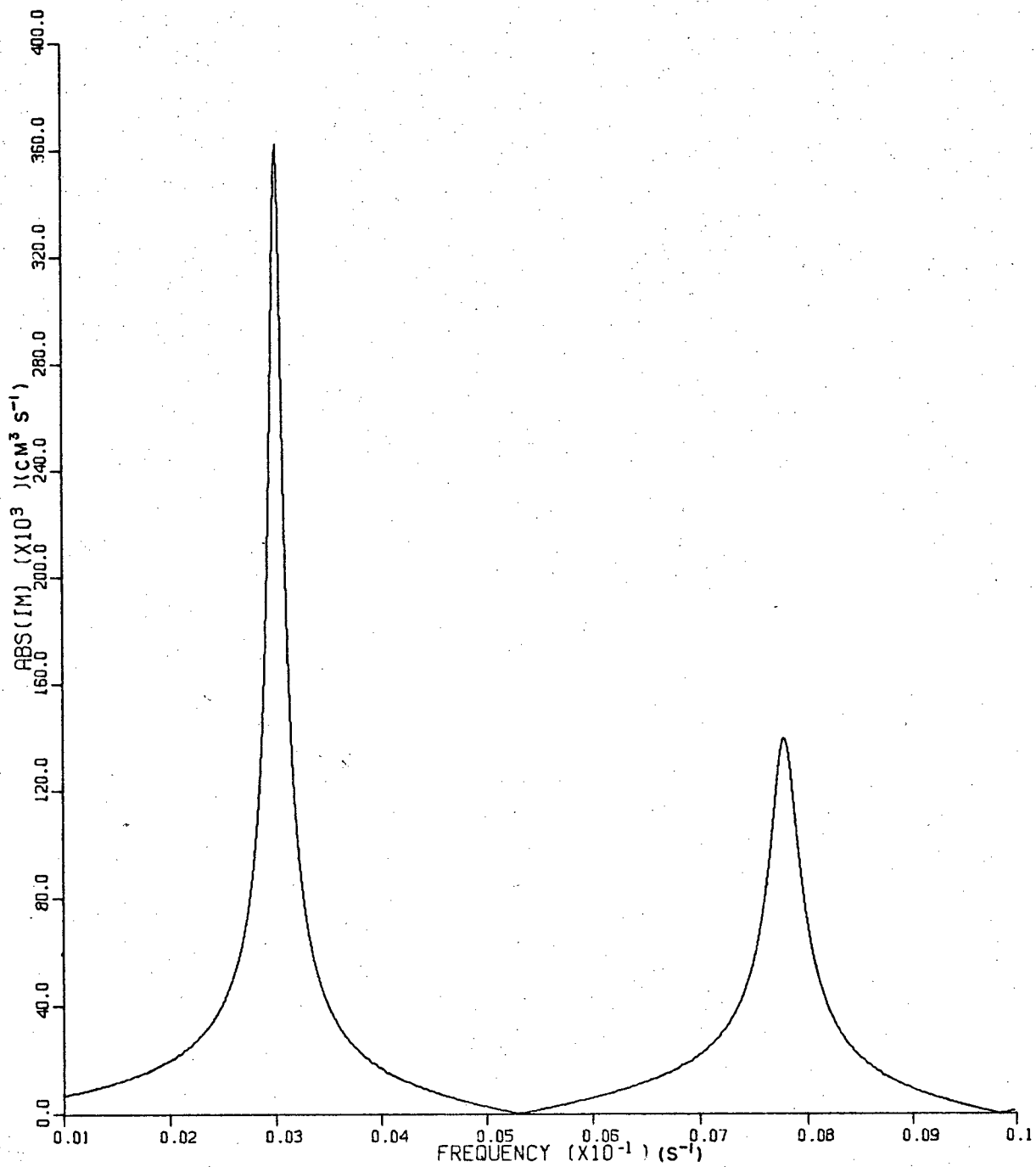

Fig. 3.5 The transport through the mouth of the bay as a function of the frequency of the forcing wave.

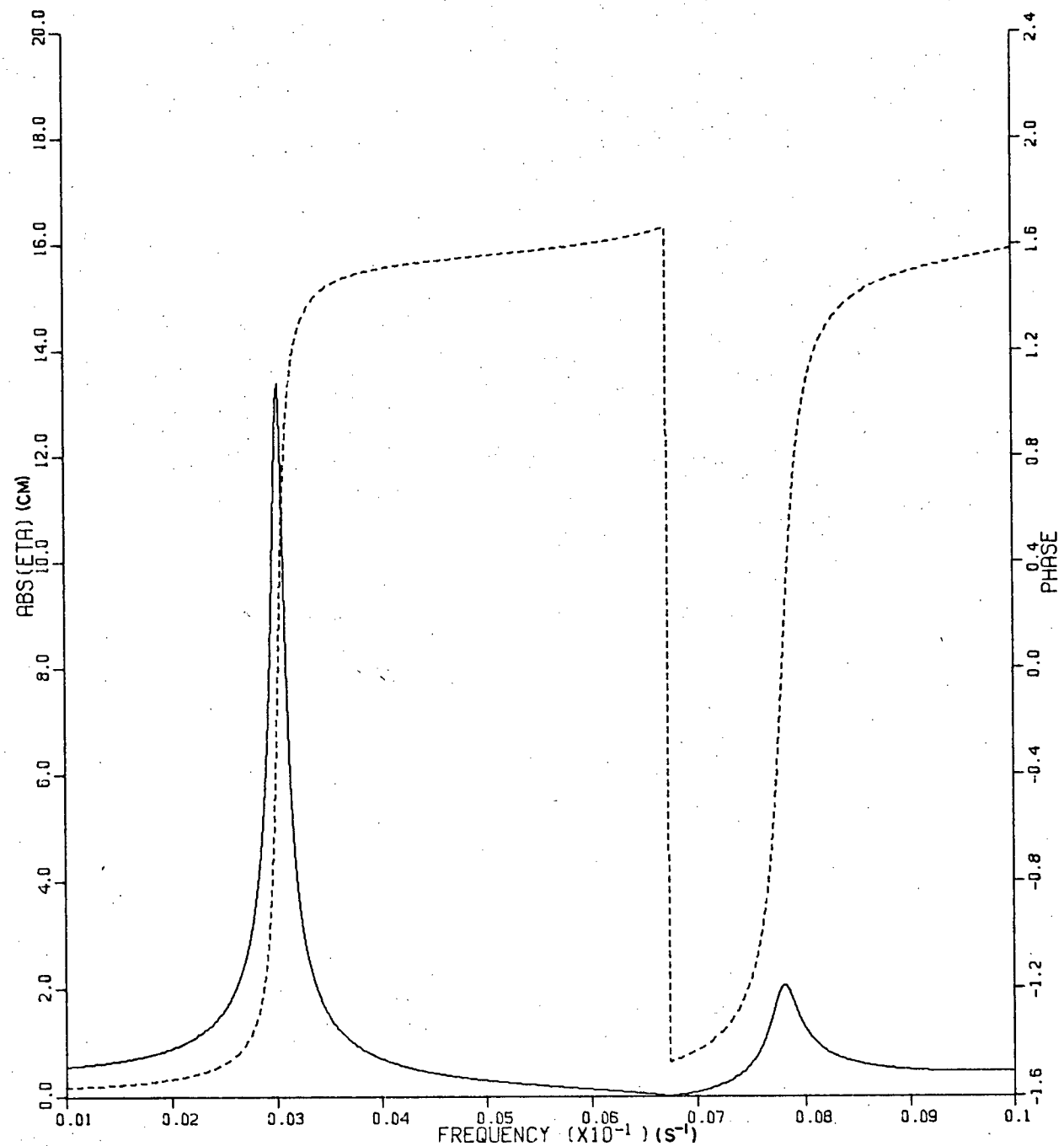

Fig. 3.6 The surface elevation (solid line) and phase relative to the forcing current (broken line) at the position of the wharf.

happens to be close to a node of the surface amplitude at that frequency (Fig. 3.8) Resonance can easily be identified from the phase curve (dotted line) as occurring at that frequency where the phase difference between the surface response and the exciting current is zero. This corresponds to a phase difference of $\pi/2$ between the surface elevation at the wharf, and that of the outside exiting wave current.

Figs. 3.7 and 3.8 show the surface configurations for the first and second modes, respectively. These plots show the absolute value of surface displacement; points where the curve touches the axis correspond to sign changes (phase changes of π). Note that in Fig. 3.8 the position of the wharf (x=2@2000mm)is near a node.

The amplification ratio A_i/A_{out} at the head of the bay is 36 for the first mode and 20 for the second mode.

4) Frictional Effects

The preceding calculations do not take into account the effects of frictional damping inside the bay. The resonance peaks in Fig. 5.5 and 5.6 are limited only by radiational damping due to the scattering of waves from the mouth of the bay.

The calculated periods are somewhat shorter than the observed periods as Table VI shows

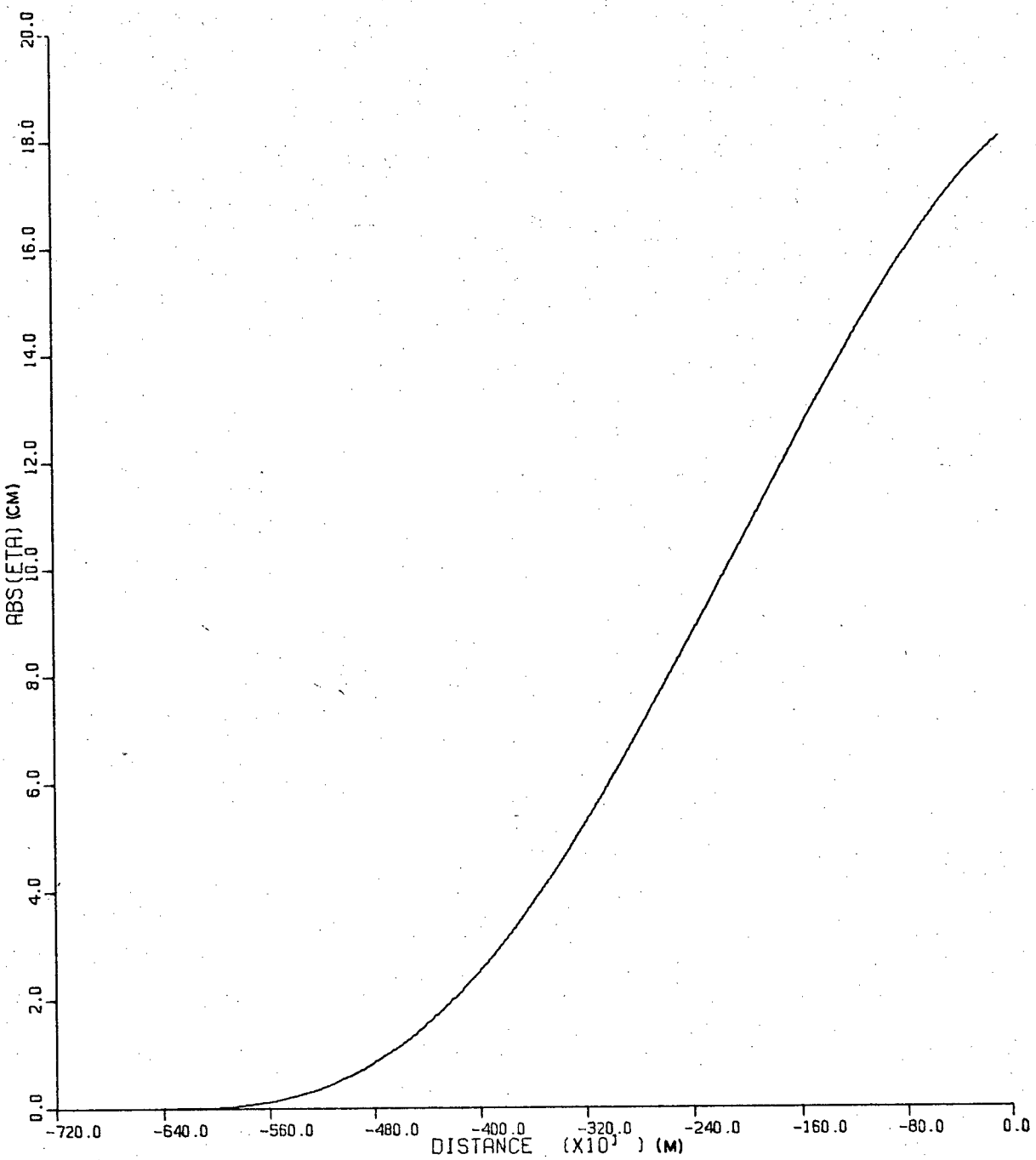

Fig. 3.7 The absolute value of the surface elevation along the bay for the fundamental mode. (The mouth is at x = -6400m. and the head is at x = 0.).

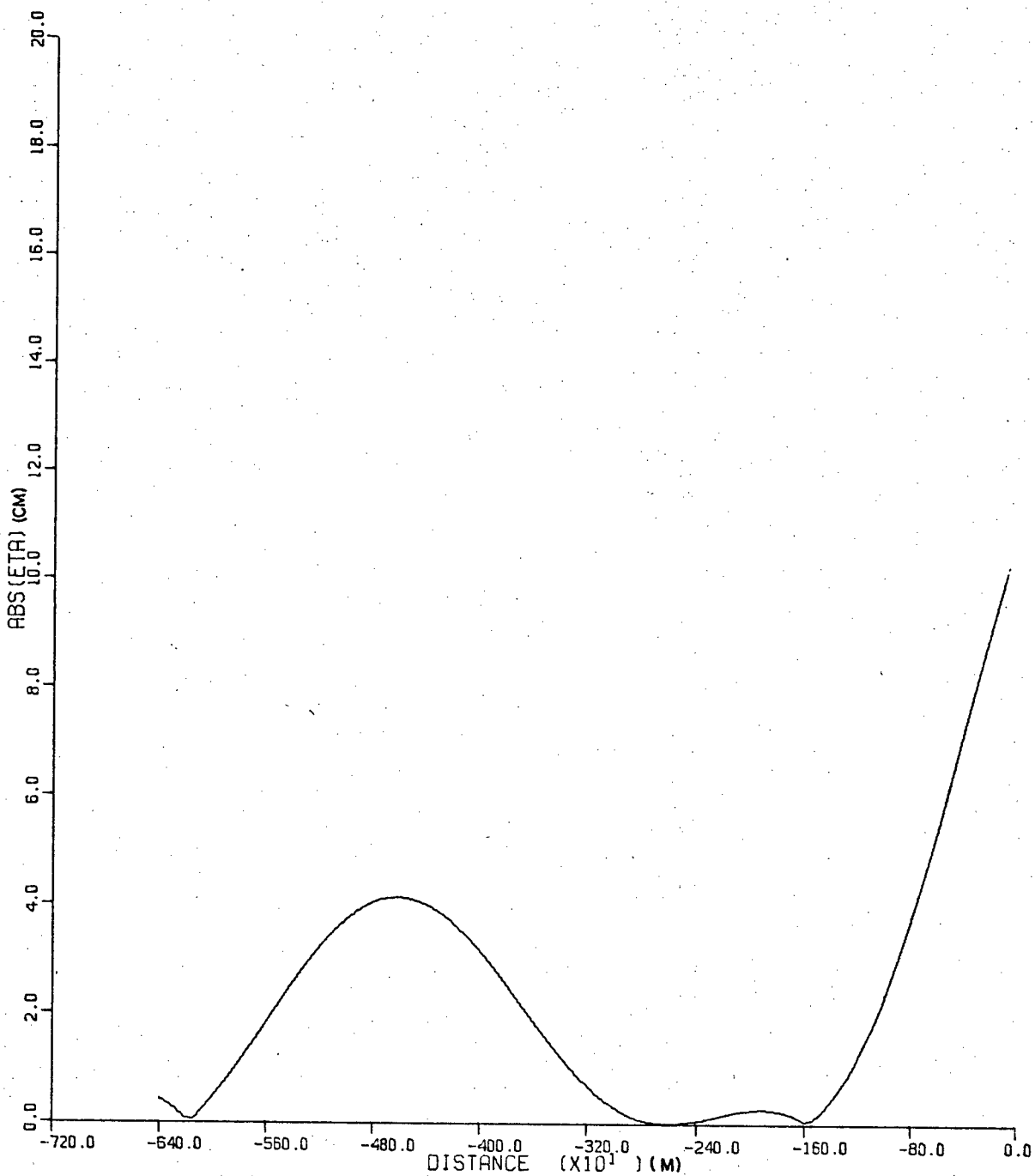

Fig 3.8 The absolute value of the surface elevation along the bay for the second mode. (The mouth is at x = -6400m: the head is at x = 0.).

Table VI

The observed and calculated seiche periods.

Mode	Calc. Period (min)	Observed Period (min)
1	$34.7 \pm .5$	38.5 ± 2
2	$13.5 \pm .5$	$14.6 \pm .6$

The effect of frictional damping may be estimated by adding an imaginary part to the frequency so that

$$\nu \rightarrow \nu + i\varepsilon$$

where ε is related to Q by

$$\varepsilon = \nu/Q$$

The inclusion of ε introduces a real part into Z_B, thereby increasing the dissipation of energy and lengthening the period. If one adds an ε equivalent to Q=1, then the calculated period is increased to $39.4 \pm .5$ min. for the fundamental mode. The amplification ratio is reduced by a factor of 2. One may calculate the value of Q necessary to bring about an overlap of the possible values of the observed and calculated periods (taking the low value of 16.5 min. for the observed wave and the high value of 35.2 min. for the calculated period), using the approximate formula for the harmonic oscillator

$$\omega_R^2 = \omega^2 - \omega_0^2/4Q^2 \qquad (3.45)$$

where ω_R is the new resonant frequency (16.5 min.) and ω_o is the frictionless resonant frequency (35.2 min.). The required Q in this case is approximately 2.5.

These values of Q are unrealistically low and compare unfavourably with the values of 10 - 20 found in Chapter 2, section 7. Realistic amounts of friction cannot account for the discrepancy between the observed and calculated results. One must conclude that, while frictional effects are important, there are other causes for this disagreement. There is probably a greater degree of radiative damping than that calculated, due to the approximations made in the calculation of the scattered waves. Geometrical effects may also be included, since the real bay does not fit the assumed model shape exactly.

CHAPTER 4:

CONCLUSIONS

An analytic model of Port San Juan as a rectangular basin with an exponentially shelving bottom predicted the first two longitudinal seiche modes to have periods of 34.7 min. and 13.5 min. Measurements taken with a bottom mounted pressure gauge showed corresponding motions at periods of 38.5 and 14.6 minutes. Other periodicities visible in the data record did not match with the theory or with other observations from the government tide gauge at Port Renfrew. These other motions are probably due to long period waves on the shelf which put energy into the bay, but do not excite it to resonance.

The theoretical response was limited only by radiational damping. Under these circumstances, the first and second longitudinal modes had theoretical Q's of 22 and 32 respectively. Measurement indicated a Q value of 10 - 15 for both modes. Addition of frictional damping to the model brought the calculated periods closer to the observed periods, however very large amounts of friction were needed to bring them into exact agreement. Such large frictional effects seem rather unrealistic; part of the discrepancy is no doubt due to friction, but the balance is more likely due to the approximations made in making a theoretical Port San Juan conform to the model.

The seiche motions are intermittent, short lived and show no obvious correlation with tides or storm activity. The most likely generating mechanism seems to be long period waves impinging on the bay entrance from outside. In the region near Port San Juan these are most likely edge waves travelling along the coast of Vancouver Island. It appears possible that they maybe excited in Imperial Eagle Channel which, because of its size, would be an efficient scatterer of larger period surface waves, and travel south along the coast into the Strait of Juan de Fuca, incidentally exciting Port San Juan on their way.

BIBLIOGRAPHY

Abramowitz, M. and Stegun, I.E. (1970) Handbook of Mathematical Functions; 7th Ed., New York: Dover Publications: 1046 pps.

Ball, F.K. (1967) Edge waves in an ocean of finite depth. Deep-Sea Research]4, 79-88.

Bendat, J.S. and Piersol, A.G. (1971) Ramdom Data: Analysis and Measurement Procedures; New York; Wiley-Interscience; 407 pps.

Bird, C., Lee,C.M. and Streat, J. (1974) U.B.C. Curve; Vancouver; University of British Columbia Computing Centre: 71 pps.

Buchwald, V.T. (1971) The diffraction of tides by a narrow channel. J. Fluid Mechanics 46, 501-511.

Defant, A. (1960), Physical Oceanography, Vol. II; New York; Pergamon Press: 598 pps.

Erdelyi, A., Magnus, W., Oberhettinger, F. and Tricomi, F.G. (1953) Higher Transcendental Functions, Vol. I; New York; McGraw-Hill 302 pps.

Froese, E. (1970) U.B.C. FOURT: Vancouver; University of British Columbia Computing Centre; 13 pps.

Galloway. J.L. (1974) Prototype of a Continental Shelf Tide Gauge; M. Sc. Thesis, University of British Columbia: 73 pps.

Garrett, C. (1975) Tides in gulfs. Deep-Sea Research 22, 23-35.

Godin, G. (1972) The Analysis of Tides; Toronto; University of Toronto Press; 264 pps.

Lathi, B.P. (1965) Signals, Systems and Communication; New York; Wiley; 607 pps.

Lautenbacher, C.C. (1970) Gravity wave refraction by islands. J. Fluid Mechanics 41, 241-265.

Murphy, G.M. (1960) Ordinary Differential Equations and Their Soutions; New York; Van Nostrand Reinhold; 541 pps.

Miles, J. W. (1971) Resonant response of harbours: an equivalent-circuit analysis. J. Fluid Mechanics 46, 241-265.

Schureman, P. (1958) Manual of Harmonic Analysis and Prediction of Tides; Special Publication 98; Washington: U.S. Dept. of Commerce-Coast and Geodetic Survey; 317 ppsl.

APPENDIX A: CROSS CHANNEL MODES

Cross-channel modes will be excited whenever the denominator in (3.27) becomes zero, i.e. if

$$\frac{\nu^2}{gh} = \frac{n^2\pi^2}{4w^2} \qquad (A1)$$

The fundamental cross-channel mode has a period of 5.17 minutes. If the outside exciting wave has a period less than or equal to 5.17 minutes then one may expect cross-channel modes to be excited. However, if this is the case, then the assumptions upon which the matching procedure in Chapter 3 is based are no longer valid. The mouth of the bay is no longer very much smaller than the wavelength of the exciting wave, and the mouth of the bay can no longer be regarded as a point source of radiation. In calculating the edge wave outside the mouth, the mouth can no longer be regarded as a negligible interruption in a long straight coast-line. The trial function $f(s)$ used in Chapter 3 can no longer take the simple form $\frac{1}{2w}$ used there; because of the cross-channel variation it must take a form close to the sinusoidal dependence of the cross-channel modes. If that is true, then it is no longer possible to have

$$\int_M f(s)\,dS = 1 \int_m f(s)\,ds = 1$$

since the flow is alternately in and out across the channel and there is no longer any net flux.

Under these circumstances, it is necessary to solve (3.23) exactly, using an exact form for the scattered wave. This necessitates solving the problem of a wave moving over a sloping bottom from an opening of finite width. This problem was beyond the scope of this thesis (for reasons described in Appendix B) and therefore the problem of cross-channel modes must remain unsolved for the time being.

APPENDIX B: GREEN'S FUNCTIONS FOR A WAVE ON A SLOPING BOTTOM

An exact form for the scattered wave moving out of the mouth of the bay requires the use of a Green's function for a wave moving from a point source out over a sloping bottom. This problem has not been solved in the literature to the best of my knowledge. This appendix offers an approach based on the treatment used by Buchwald (Buchwald, 1971) but derives only an integral form for the Green's function, not a closed expression.

Assume topography and coordinate axes identical to those used for the edge waves in Ch. 3. Let the free edge wave travelling along the coast be denoted by $F_m(x)e^{i(\nu t - my)}$ where m stands for the wave number. Assume that the frequency involved is sufficiently high to neglect rotation. Let there be a point source of current at (0,0)

$$U(o,y) = \delta(y)\, e^{i\nu t}$$

Then one may express the surface elevation at any point in the ocean in the following integral form (Buchwald, 1971)

$$\eta_G = \int_{-\infty}^{\infty} \Phi(m)\, e^{-imy}\, F_m(x)\, e^{i\nu t}\, dm \quad , \tag{B1}$$

and the velocity field as

$$i\nu u = -g \int_{-\infty}^{\infty} \Phi(m)\, e^{-imy}\, F_m'(x)\, e^{i\nu t}\, dm \; . \tag{B2}$$

At the coast (x = 0), these expressions take the form

$$i\nu\delta(y) = -g\int_{-\infty}^{\infty} \Phi(m)\, e^{-imy}\, F_m'(0)\, dm \,, \tag{B3}$$

$$hk^2\delta(y) = \int_{-\infty}^{\infty} i\nu\Phi(m)\, e^{-imy}\, F_m'(0)\, dm \,. \tag{B4}$$

Applying Fourier's inversion theorem:

$$i\nu\Phi(m)\, F_m'(0) = hk^2/2\pi \,.$$

Then, the expression for η_G, which is the Green's function desired, is

$$\eta_G = \int_{-\infty}^{\infty} \frac{ihk^2}{2\pi\omega} \frac{F_m(x)}{F_m'(0)} e^{-imy}\, dm \,,$$

$$= \frac{-i}{2\pi g} \int_{-\infty}^{\infty} \nu(m) \frac{F_m(x)}{F_m'(0)} e^{-imy}\, dm \,. \tag{B5}$$

Equation (3.17) gives the form of $F_m(x)$ for edge waves such as are considered here:

$$F_m(x) = A\, e^{pbx} \frac{\Gamma(2p+1)}{\Gamma(-n)\Gamma(n+2p+1)} \sum_{j=o}^{n} \frac{\Gamma(j-n)\,\Gamma(2p+1+j+n)\, e^{-jcx}}{\Gamma(2p+1+j)\, j!} \,.$$

The derivative, $F_m'(x)$, has the form

$$F_m'(x) = p + \sum_{j=0}^{n} (p+n) a_j\, (\pm 1)^j \,,$$

where a_j is an abbreviation for

$$a_j = \frac{\Gamma(2p+1)}{\Gamma(2p+n+1)} \frac{\Gamma(2p+n+j+1)}{\Gamma(2p+j+1)} \cdot$$

The expression for the Green's function η_G then becomes

$$\eta_G(x) = \frac{i\nu}{2\pi gb} \sum_{n=0}^{\infty} \int_{-\infty}^{\infty} \frac{e^{-pbx} \left[1 + \sum_{j=1}^{n} a_j e^{-jcx} (-1)^j\right] e^{-imy}}{\left[p + \sum_{j=0}^{n} (p+n)(-1) a_j\right]} dm \quad (B6)$$

This integral must be evaluated for every possible value of n and the results summed in order to express completely η_G. This appears to be impossible to perform, since reference to 5.14 will show that both the a_i and p contain m, the variable of integration.

In practice, it may be possible to expand the integrand for the first few values of n, thereby finding an approximation to η_G.

For example, if n=o then $F_m(x) = A\, e^{pcx}$ and $p = \sigma^2$ and the expression for η_G reduces to

$$\eta_G(x) = \frac{i\nu}{2\pi gb} \int_{-\infty}^{\infty} \frac{\exp[-\nu^2 x/gh_o b]\, e^{-imy}}{\nu^2/gh_o b^2} dm \quad , \quad (B7)$$

which is very similar to the result for the case of a flat bottom:

$$\eta_f(x) = \frac{ihk^2}{2\pi} \int_{-\infty}^{\infty} \frac{e^{-imy - sx}}{\nu s} dm \quad , \quad (B8)$$

where $s' = \sqrt{m^2 - k^2}$. Higher order terms become progressively more complicated. However, the forms of (B7) and (B8) are quite similar, which means that the flat-bottom approximation is not bad, especially as the fundamental (n=0) edge wave mode is the most easily stimulated (Ball, 1971).

APPENDIX C: THE INSTRUMENT

The general requirements that the instrument had to satisfy were that it should be portable, capable of measuring small surface elevations with high accuracy and that it should be capable of resolving frequencies from surface waves to tides: a period range of 1 second to 24 hours. A short summary of the operation of the instrument is given here; those interested in a detailed description should refer to Galloway (1974).

The instrument consisted of 3 stages: a pressure transducer, a digital processing section, and an analogue output section. The pressure transducer was a vibrotron, mounted together with a preamplifier in a pressure casing. The vibrotron was a shallow water model, capable of measuring pressures up to 25 psi (17.3 KPa). Its output is a sinusoidal oscillation whose frequency depends on pressure in the following manner

$$F_v^2 = -aP + b \qquad (C.1)$$

with a sensitivity

$$\frac{dF_v}{dz} = -35 \text{ Hz/ft} \qquad (C.2)$$

and a centre frequency of 14.5 KHz. The vibrotron signal is transmitted up a cable to a waveshaper which converts the sinusoidal signal to a square wave of the same frequency.

The signal is then passed to 4 channels inside the instrument

for measurement of frequency (with the aid of a crystal oscillator as a reference clock). These 4 channels are divided into 2 groups: 2 high sampling rate channels and 2 low sampling rate channels. The high frequency channels were sampled every 0.5 sec. (i.e. at a sampling frequency of 2 Hz.) in order to resolve the surface wave spectrum; the low frequency channels were sampled every 21 sec. (0.048 Hz.) and a running mean was performed in between in order to filter partially the surface waves. (The effect of a 21 second average would reduce the effective surface wave amplitude by a factor of 10.) Each of these groups contained a high and low resolution channel; the high resolution channels utilized the wraparound technique of scale expansion described in Ch. 2 Section 2 while the low resolution channels did not. The low resolution channels were included in case the wraparounds could not be removed from the data afterwards. It did not prove necessary to use them as the wraparounds were removed successfully.

These four signals are written as digital numbers into four buffers on each sampling. The contents of the buffers are then written via four digital to analogue (D/A) converters onto a four track F.M. tape recorder (Hewlett-Packard). When the data was taken at Port Renfrew the channels were set as follows:

Low Frequency	High Resolution:	0.43 metres full scale
		1.70 mm. sensitivity
	Low Resolutions:	6.97 metres full scale
		27.2 mm. sensitivity

	High Resolution:	0.83 metres full scale
High Frequency		3.23 mm. sensitivity
	Low Resolution:	6.62 metres full scale
		25.8 mm. sensitivity

The D/A converters worked in the range -5v. to +5v. with an error of $\pm$ 5 mv.

The major source of noise in the instrument is the tape recorder, which has a noise level of 10 mv. rms. This, together with the D/A converters contributed all the significant noise. For the most sensitive channels, this means a random variation of 0.43 mm. and 0.83 mm. for the low and high frequency channels respectively. In each case this represents about 30% of the smallest detectable variation, and therefore is not significant.